



HHS Public Access

Author manuscript

Immunity. Author manuscript; available in PMC 2023 November 15.

Published in final edited form as:

Immunity. 2023 July 11; 56(7): 1631–1648.e10. doi:10.1016/j.immuni.2023.06.007.

TCR-independent CD137 (4–1BB) signaling promotes CD8⁺ exhausted T cell proliferation and terminal differentiation

Andrea C. Pichler^{1,2,9}, Nadège Carrié^{1,9}, Marine Cuisinier^{1,3,9}, Samira Ghazali⁴, Allison Voisin⁵, Pierre-Paul Axisa¹, Marie Tosolini¹, Céline Mazzotti^{1,3}, Dominic P. Golec², Sabrina Maheo^{1,3}, Laura do Souto^{1,3}, Rüçhan Ekren¹, Eve Blanquart¹, Lea Lemaitre¹, Virginie Feliu¹, Marie-Véronique Joubert^{1,3}, Jennifer L. Cannons², Camille Guillerey⁶, Hervé Avet-Loiseau^{1,3}, Tania H. Watts⁷, Benoit L. Salomon^{4,8}, Olivier Joffre⁴, Yenkel Grinberg-Bleyer⁵, Pamela L. Schwartzberg², Liliana E. Lucca^{1,*}, Ludovic Martinet^{1,3,10,*}

¹Cancer Research Center of Toulouse (CRCT), Institut National de la Santé et de la Recherche Médicale (INSERM), Centre National de la Recherche Scientifique (CNRS), Université Toulouse III-Paul Sabatier (UPS), Toulouse, France

²Cell Signaling and Immunity Section, Laboratory of Immune System Biology, National Institute of Allergy and Infectious Diseases, National Institutes of Health, Bethesda, MD, USA

³Institut Universitaire du Cancer, CHU Toulouse, Toulouse, France

⁴Toulouse Institute for Infectious and Inflammatory Diseases (Infinity), UPS, INSERM, CNRS, Toulouse, France

⁵Centre de Recherche en Cancérologie de Lyon, Labex DEVweCAN, INSERM, CNRS, Université Claude Bernard Lyon 1, Centre Léon Bérard, Lyon, France

⁶Cancer Immunotherapies Group, The University of Queensland, Brisbane, QLD, Australia

⁷Department of Immunology, University of Toronto, Toronto, ON M5S 1A8, Canada

⁸Sorbonne Université, INSERM, CNRS, Centre d'Immunologie et des Maladies Infectieuses (CIMI-Paris), Paris, France

⁹These authors contributed equally

¹⁰Lead contact

SUMMARY

This is an open access article under the CC BY-NC-ND license (<http://creativecommons.org/licenses/by-nc-nd/4.0/>).

*Correspondence: liliana.lucca@inserm.fr (L.E.L.), ludovic.martinet@inserm.fr (L.M.).

AUTHOR CONTRIBUTIONS

Study conception and design, A.C.P., N.C., and L.M.; acquisition of data, A.C.P., N.C., M.C., A.V., C.M., D.P.G., S.M., L.L., V.F., M.-V.J., and C.G.; analysis and interpretation of data, A.C.P., N.C., A.V., P.-P.A., M.T., L.d.S., O.J., Y.G.-B., L.E.L., and L.M.; drafting of manuscript, A.C.P., P.L.S., L.E.L., and L.M.; critical revision and editing, A.C.P., R.E., E.B., J.L.C., H.A.-L., T.H.W., B.L.S., O.J., Y.G.-B., P.L.S., L.E.L., and L.M.; provision of key materials, T.H.W., B.L.S., P.L.S., H.A.-L., and L.M.

DECLARATION OF INTERESTS

The authors declare no competing interests.

SUPPLEMENTAL INFORMATION

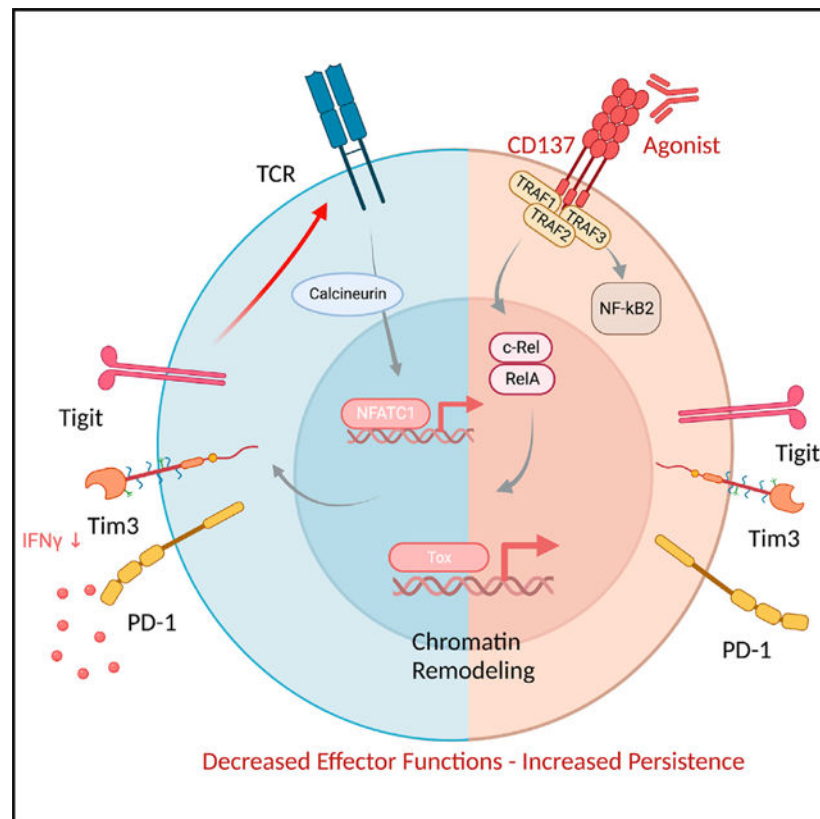
Supplemental information can be found online at <https://doi.org/10.1016/j.immuni.2023.06.007>.

CD137 (4–1BB)-activating receptor represents a promising cancer immunotherapeutic target. Yet, the cellular program driven by CD137 and its role in cancer immune surveillance remain unresolved. Using T cell-specific deletion and agonist antibodies, we found that CD137 modulates tumor infiltration of CD8⁺-exhausted T (Tex) cells expressing PD1, Lag-3, and Tim-3 inhibitory receptors. T cell-intrinsic, TCR-independent CD137 signaling stimulated the proliferation and the terminal differentiation of Tex precursor cells through a mechanism involving the RelA and cRel canonical NF- κ B subunits and Tox-dependent chromatin remodeling. While Tex cell accumulation induced by prophylactic CD137 agonists favored tumor growth, anti-PD1 efficacy was improved with subsequent CD137 stimulation in pre-clinical mouse models. Better understanding of T cell exhaustion has crucial implications for the treatment of cancer and infectious diseases. Our results identify CD137 as a critical regulator of Tex cell expansion and differentiation that holds potential for broad therapeutic applications.

In brief

Manipulating exhausted T (Tex) cells has therapeutic implications. Pichler et al. found that the activating receptor, CD137 (4–1BB), was specifically expressed by Tex cells. CD137 signaling promoted TCR-independent proliferation and terminal differentiation of Tex cells. In murine tumor models, treatment with CD137 agonists specifically after anti-PD1 therapy improves anti-tumor responses.

Graphical Abstract



INTRODUCTION

Co-inhibitory receptors, such as PD1, Tim3, Lag-3, TIGIT, and CTLA-4 play a key role in driving a state of CD8⁺ T cell hyporesponsiveness called T cell exhaustion, that is frequently observed in chronic viral infections and cancer.¹ Although, exhausted T (Tex) cells represent a unique T cell lineage, “T cell exhaustion” is a general term that includes various distinct epigenetic and metabolic states associated with effector T cell dysfunction.^{2–5} Several transcription factors (TFs) regulate Tex cell program including Eomes, TCF-1,^{6–10} and the high-mobility group (HMG) protein Tox.^{11–13} The latter is required for the epigenetic remodeling and survival of exhausted CD8⁺ T cells.^{11,12,14,15} Prolonged T cell receptor (TCR) signaling due to persistent antigen exposure seems to represent a cardinal cause of exhaustion in chronic infection and cancer.¹⁶ However, additional signals may also participate in exhaustion program since the mechanisms impacting Tex cell differentiation are still poorly understood.^{9,17–19}

Targeting T cell exhaustion is a promising therapeutic strategy against cancer as illustrated by the clinical success achieved with monoclonal antibodies (mAbs) blocking PD1 and CTLA-4.^{20,21} Still, these immune checkpoint blockers (ICBs) may only reinvigorate a subset of Tex cells with a progenitor or stem-like signature and the clinical responses are observed only in a fraction of cancer patients.^{22,23} Therefore, finding alternatives to increase ICB efficacy is being actively pursued. Most current strategies target additional inhibitory receptors, but activating receptors may also impact the efficacy of cancer immunotherapy as recently evidenced for CD226 (DNAM-1).^{24–26}

CD137 (TNFRSF9, 4–1BB) is a costimulatory member of the tumor necrosis factor receptor (TNFR) superfamily, expressed by activated T cells and other cells.²⁷ The engagement of CD137 with its natural ligand CD137L (4–1BBL, TNFSF9) on activated dendritic cells (DCs) enhances T cell proliferation and cytokine secretion and protects T cells from activation-induced cell death.^{28–30} CD137 stimulation expands CD8⁺ effector memory T (Tem) cells and promotes tumor regression in diverse mouse models.^{31–33} CD137 hence represents a promising immunotherapeutic target against cancer. Yet, anti-CD137 mAbs such as urelumab had limited efficacy and showed liver toxicity in early-phase clinical trials.^{34,35} In addition, the mechanisms underlying the anti-tumor vs. the immune regulatory activity of anti-CD137 agonists are largely unexplained. Indeed, anti-CD137 agonists decrease clinical symptoms in several mouse models of autoimmunity, suggesting that the CD137 stimulation may dampen immune responses.^{36–39} Thus, there is a clear need to better understand the cellular programs driven by CD137 receptor stimulation.

In this study, using T cell-specific CD137-deficient mice and different tumor models, we found that CD137 absence limited the accumulation of tumor-infiltrating Tex cells. Through single-cell transcriptomic, epigenomic, and functional analysis, we demonstrated that NF- κ B-dependent CD137 signaling induces the TCR-independent expansion of CD8⁺ T cells already committed into Tex cell program. Our results uncovering the role of CD137 signaling in T cell exhaustion may have broad therapeutic implication in chronic infectious disease and cancer as shown by the ability of CD137 agonists to improve anti-PD1 efficacy in our pre-clinical mouse models.

RESULTS

CD137 deficiency limits tumor-infiltrating Tex cells

To address the role of CD137 in CD8⁺ T cell anti-tumor surveillance, we crossed *Cd137^{fl/fl}* mice with *Cd4^{cre}* mice, specifically deleting CD137 expression in the T cell compartment. *Cd4^{Cre}Cd137^{fl/fl}* and *Cd137^{fl/fl}*, referred to as *Cd137^{-/-}* and *Cd137^{+/+}* mice, respectively, were injected s.c. with MC38 colon carcinoma cells or B16K1 melanoma cells (Figure 1A), two CD8⁺ T cell-dependent immunogenic tumor models.^{24–26} CD137 deficiency resulted in higher tumor burden at later time points in both B16K1 and MC38 mouse models suggesting that the absence of CD137 negatively impacts T cell anti-tumor immune response (Figure 1A). Indeed, CD137 deficiency decreased the frequency and number of CD8⁺ tumor-infiltrating T lymphocytes (TILs) in these tumor models (Figures 1B and S1A). B16K1 or MC38-CD8⁺ TIL phenotypic differences were also observed with a reduction in PD1- and Tim3-expressing CD8⁺ TILs in *Cd137^{-/-}* mice compared with *Cd137^{+/+}* counterparts (Figures 1C and S1A). Nonetheless, splenic CD8⁺ T cell numbers and phenotypes were similar between tumor-bearing *Cd137^{-/-}* and *Cd137^{+/+}*-mice, and CD137 deficiency did not alter T cell homeostasis in naive mice (Figure S1B).

To exclude any impact of CD137 deletion on other T cell subsets, we generated mixed hematopoietic bone marrow (BM) chimeras. Lethally irradiated C57BL/6 mice reconstituted with *Cd4^{cre}Cd137^{fl/fl}ROSA26^{tomato}* (*Cd137^{-/-}*; tomato⁺) and *Cd137^{fl/fl}ROSA26^{tomato}* (*Cd137^{+/+}*; tomato⁻) donor BM cells were injected with B16K1 cells (Figure 1D). We observed an increase in the ratio of *Cd137^{+/+}* vs. *Cd137^{-/-}* (CD137^{WT/KO}) CD8⁺ T cell in the tumor microenvironment as compared with the spleen (Figure 1D), resulting in higher numbers of *Cd137^{+/+}* than *Cd137^{-/-}* CD8⁺ T cells within tumor lesions (Figures S1C and S1D). The frequency and number of *Cd137^{-/-}* CD8⁺ TILs expressing PD1 and Tim3 were also reduced compared with *Cd137^{+/+}* counterparts (Figures S1C and S1D). These results were confirmed using *Cd137^{+/+}* and *Cd137^{-/-}* CD8⁺ T cells transferred into lymphopenic *Rag2^{-/-}Il2rg^{-/-}* mice injected with B16K1 cells suggesting a CD8⁺ T cell-intrinsic impact of CD137 on T cell exhaustion (Figures S1E and S1F). To confirm these results at the molecular level, we performed a single-cell RNA sequencing (scRNA-seq) analysis of spleen and tumor CD8⁺ T cells isolated from *Cd137^{-/-}* and *Cd137^{+/+}* mixed chimeras bearing B16K1 tumor (Figure 1E). The transcriptomic landscape of splenic CD8⁺ T cells was similar between *Cd137^{+/+}* and *Cd137^{-/-}* and was mostly composed of cell clusters expressing naive and memory T (Tmem) cell signature genes (*Ccr7*, *Sell*, and *Tcf7*) (Figures 1F–II and S1G). By contrast, the difference between *Cd137^{+/+}* and *Cd137^{-/-}* transcriptomic profiles was more profound in CD8⁺ TILs (Figures 1H, 1I, and S1H). The Tex cell cluster that was enriched in expanded clonotypes (Figures S1I and S1J) and expressed *Tnfrsf9*, *Pdcd1*, *Tigit*, *Tox*, and Tex cell signatures (Figures 1F and 1G) was the most abundant in *Cd137^{+/+}* TILs. This cluster was decreased among *Cd137^{-/-}* TILs that were enriched in clusters expressing central memory T (Tcm) cells and activated T cell signature genes (Figures 1F–II, S1G, and S1H). GSEA, performed on *Cd137^{+/+}* and *Cd137^{-/-}* CD8⁺ TIL differentially expressed genes, confirmed that *Cd137^{+/+}* TILs were enriched in chronic lymphocytic choriomeningitis virus (LCMV) infection and cancer exhaustion signatures,^{11,13,19,22,40,41} while *Cd137^{-/-}* TILs were enriched in cancer-associated Tmem

cell signatures^{42–46} (Figure 1J). Together, these results confirm that the absence of CD137 affects the presence of Tex cells within tumor lesions.

CD137 expression was restricted to tumor-infiltrating PD1⁺ Tem (CD62L⁻CD44^{hi}) cells upon tumor development (Figure 1K). A more detailed analysis revealed that terminal Tex cells (TermTex; PD1⁺TCF1⁻Tim3⁺) displayed a higher CD137 expression than progenitor Tex cells (Tpex; PD1⁺ TCF1⁺Tim3⁻) (Figure 1K). Accordingly, TermTex cells were the more affected subset by the absence of CD137 while Tpex CD137^{WT/KO} ratios were only mildly increased compared with PD1⁻ counterparts (Figure 1L). In contrast, the ratios of CD137^{WT/KO} naive T cells (Tn, CD62L⁺CD44^{low}) and Tcm cells (CD62L⁺CD44^{high}) were similar in mixed chimeras among the spleen, draining lymph node (DLN), and tumor, consistent with their very-low CD137 expression (Figures 1K and 1L). Analysis of public datasets of CD8⁺ TIL scRNA-seq from human melanoma⁴⁷ and breast cancer⁴⁸ confirmed the higher expression of *TNFRSF9* on Tex cell clusters (Figures S1K and S1N). *TNFRSF9* expression strongly correlated with terminally Tex cell genes *HAVCR2*, *TIGIT*, and *TOX* (Figure S1L). Reciprocally, *in silico*-gated *TNFRSF9*-expressing TILs had a higher Tex cell signature⁴⁹ than *TNFRSF9* negative TILs (Figures S1M and S1O). Together, these data showed the specific expression of CD137 on tumor-infiltrating CD8⁺ Tex cells. Furthermore, the reduction of this subset in the absence of CD137 receptor suggests a role for this receptor in Tex cell accumulation within tumors.

CD137 stimulation favors tumor Tex cell accumulation

To address whether CD137 signaling favors Tex cell accumulation in the tumor, we analyzed the impact of CD137 stimulation on tumor associated CD8⁺ T cells using a well-described anti-CD137 agonist mAb (clone 3H3).³⁰ WT mice bearing detectable B16K1 tumors were injected with control Ig or anti-CD137 mAbs, and the TIL composition was analyzed (Figure 2A). Anti-CD137 treatment increased the frequency and number of CD8⁺ T cells expressing PD1 and Tim3 markers compared with Ig-treated controls, while PD1⁻ Tmem TIL numbers remained stable (Figures 2B and 2C). This increase in Tex cells induced by anti-CD137 treatment was negligible in *Cd137*^{-/-} mice (Figures 2B and 2C). To address the impact of CD137 agonists on tumor antigen-specific TILs, CD8⁺ T cells from OT-1 mice, which express a transgenic TCR recognizing a peptide from ovalbumin (ova) in the context of major histocompatibility complex (MHC) class I, were transferred into B16-ova-bearing *Cd45.1* mice and treated with Ig or anti-CD137 (Figure 2D). Anti-CD137 increased the frequency and the number of exhausted PD1⁺Tim3⁺ OT-1 cells infiltrating B16-ova tumors as compared with Ig treatment (Figure 2D). Thus, CD137 agonism enhances the exhaustion program in exhaustion prone immunogenic solid tumor models.

In the VK12653 mouse model of myeloma, which develops in the BM and does not induce strong T cell exhaustion,^{33,53} anti-CD137 treatment induced the expansion of CD8⁺ T cells co-expressing the inhibitory receptors PD1, Tim3, TIGIT, and Lag-3 and the TFs Tox and Eomes (Figures S2A and S2B). A kinetic scRNA-seq analysis of CD8⁺ T cells infiltrating VK12653 lesions treated with anti-CD137 or control Ig confirmed these findings (Figures 2E–2J and S2C). Indeed, most TILs from Ig controls and early-stage anti-CD137 treatment (day 1 and day 4) were located in cluster C1 and expressed Tn genes (*Ccr7*,

Ii7r, and *Sell*) (Figures 2H–2J, S2D, and S2E). In contrast, TILs from day 11 and day 18 anti-CD137 condition were located in clusters C2–C4 and were characterized by the expression of tumor and LCMV Tex cell signatures^{40,41,50,51} and genes (Figures 2G–2J, S2D, and S2E). Cluster 2 had features of T_{pex} cells (*Tcf7*, *Cxcr5*, and *Slamf6*) while cluster 3 had proliferating and effector-like Tex cell features (*Top2a*, *Hmgb2*, *H2afz*, *Tbx21*, *Cxcr3*, and *Klrg1*) (Figure 2J). Both clusters peaked by 11 days of anti-CD137 (Figure 2I). Cluster 4 was enriched in TermTex genes (*Lag3*, *Havcr2*, *Pdcd1*, and *Tox*) and represented most of the TILs after 18 days of anti-CD137 (Figures 2I and 2J). Comparison of our scRNA-seq data that from chronic (C113) or acute (Arm) LCMV and tumor-specific CD8⁺ T cell datasets^{10,41,52} confirmed that day 11 and day 18 anti-CD137 TILs shared important similarities with chronic infection and tumor Tex program (Figures 2K–2M, S2F, and S2G). *Tnfrsf9* expression was only visible on chronic LCMV and tumor Tex cell clusters but not acute LCMV effectors (Figure 2L). Together, these data demonstrate that anti-CD137 agonists induce the accumulation of CD8⁺ T cells characterized by a Tex cell transcriptomic program.

CD137 promotes Tex cell expansion and differentiation

We found that anti-CD137 mAbs induced Tex cell accumulation not only in the tumor but also in all the lymphoid organs tested even in the absence of tumors (Figures S3A–S3C). These PD1⁺ and Tim3⁺ CD8⁺ Tem cells that accumulated in naive mice upon CD137 stimulation had decreased ability to proliferate and produce IL-2, IFN- γ , and TNF compared with PD1⁻ and Tim3⁻ counterparts confirming their functional exhaustion (Figures S3D and S3E). Similar results were obtained with a different CD137 agonist (clone LOB12.3, Rat IgG1) with a lower affinity, a different isotype and whose mechanism of action requires Fc γ R cross linking⁵⁴ (Figure S3F). Increased expression of PD1 and Tim3 by CD8⁺ Tem cells in non-tumor-bearing mice was also evident with low doses of CD137 agonists (Figure S3G). These results indicate that CD137 stimulation leads to a systemic Tex-cell-promoting effect, independent of tumor or chronic infection. We therefore questioned the mechanisms involved.

CD137 has been implicated in T cell survival,^{55,56} but we did not observe differences in the expression of active caspase 3/7 among *Cd137*^{+/+} and *Cd137*^{-/-} CD8⁺ TILs (Figure S3H). In addition, anti-CD137 treatment did not affect the level of CD8⁺ T cells apoptosis suggesting that decreased apoptosis may not explain the Tex-cell-promoting effect of CD137 (Figure S3I). CD137 has also been suggested to represent a growth factor for Tmem cells.³² Accordingly, anti-CD137 treatment quickly increased Ki67 expression in PD1⁻ CD44^{hi} CD8⁺ Tmem cells in WT mice (Figures 3A and 3B). Ki67 expression was primarily restricted to PD1⁺CD44⁺ memory CD8⁺ T cells upon CD137 stimulation (Figures 3A and 3B). The proliferation of both T_{pex}-like (PD1⁺TCF1⁺Tim3⁻) and TermTex-like (PD1⁺TCF1⁻Tim3⁺) phenotype cells was increased upon CD137 stimulation compared with naive and PD1⁻ Tmem cells (Figures 3C and 3D). This suggests that CD137 specifically triggers the expansion CD8⁺ T cells with a Tex cell phenotype even in naive mice. Indeed, accumulating evidence supports the progressive expansion in “specific-pathogen-free” (SPF) mice, with age, of CD8⁺ T cells with Tex-like features including PD1⁺ and Tim3⁺ expression and functional defects, probably reactive to commensal/endemic

pathogens or self-antigens.^{57–59} To address this question, we sorted naive (Tn, CD44⁻CD62L⁺), memory (Tmem, PD1⁻CD44^{hi}), and PD1⁺ (Tex-like CD44^{hi}PD1⁺) cells from *Cd45.1* mice and transferred them into *Cd137*^{-/-} mice whose T cells do not respond to CD137 agonists (Figure 3E). The percentages of CD45.1 Tn and Tmem cells recovered after 2 weeks were very low for both conditions, while CD45.1 PD1⁺ Tex-like cells were increased by anti-CD137 treatment (Figure 3F). To confirm the differential impact of CD137 stimulation on CD8⁺ T cell subsets, we performed a scRNA-seq analysis of PD1⁻ (Tmem), PD1⁺SLAMF6⁺Tim3⁻ (Tpex-like), and PD1⁺SLAMF6⁻Tim3⁺ (Tex-like) splenic CD44^{hi}CD8⁺ T cells isolated from WT mice treated with anti-CD137 mAbs or rare cells expressing the same markers in the Ig-treated controls (Figures 3G and S3J). The composition of PD1⁻ Tmem cells was almost similar between Ig and CD137 conditions, once again suggesting the lack of impact of CD137 engagement on these PD1⁻ Tmem cell subsets (Figures 3H and 3I). They were composed mainly of clusters C0 and C2 with naive and central Tmem cell signature genes and had almost undetectable *Tnfrsf9* expression (Figures 3H, 3I, and S3K). Tpex-like cells from Ig and CD137 treated mice were also quite similar except a small cluster of *Tnfrsf9*-expressing cells (C5), characterized by proliferating and progenitor-exhausted signatures that expanded in CD137-treated mice (Figures 3H–3J and S3K). The main differences between Ig and anti-CD137 conditions were observed for the Tex-like cell subsets (Figures 3H and 3I). Most of the Ig Tex-like cells belonged to cluster 3, with a mixed signature of pre-exhausted, effector-like, and proliferating Tex cells while, in the anti-CD137 condition, these cells belonged to cluster 4, mainly characterized by chronic LCMV and tumor TermTex signature genes (Figures 3H, 3I, and S3K). The canonical signatures and genes related to Tex cell terminal differentiation (e.g., *Pdcd1*, *Havcr2*, *Nr4a2a*, and *Lag3*) that were already expressed by Tex-like cells in the Ig condition were further increased upon anti-CD137 treatment (Figures 3K, 3L, and S3L). Projection of our scRNA-seq with Giles et al.⁵² confirmed these findings (Figures S3N and S3M). We further validated the differential effect of CD137 engagement on PD1⁻ Tmem, Tpex, and Tex cells by transferring these subsets into *Rag2*^{-/-}*Il2rg*^{-/-} mice that were subsequently treated with anti-CD137 mAbs (Figure 3M). Tpex and Tex cell numbers were higher upon anti-CD137 treatment compared with Ig controls while PD1⁻ Tmem cell numbers did not differ (Figure 3N). In addition, PD1⁻ Tmem cells did not acquire a Tpex or TermTex phenotype upon anti-CD137 treatment while most of the Tpex-like cells acquired a TermTex phenotype characterized by PD1 and Tim3 expression (Figures 3O and 3P). Together these results indicate that CD137 stimulation induces the expansion of memory CD8⁺ T cells that are already committed into a Tex cell program and favors their differentiation into terminally differentiated Tex cells.

CD137-induced Tex cell expansion does not require TCR/calcineurin signaling pathway

Our results showing that CD137 engagement promotes the proliferation and the differentiation of Tex cells, even in naive mice, raised the question of the role of TCR signaling in this effect. To date, TCR-induced calcineurin-NFAT signaling is the main—if not the only—identified driver of T cell exhaustion.^{11,60} Yet, anti-CD137 agonism induced the expansion of Tex cells upon transfer of OT-1 cells into WT mice in the absence of ova antigen (Figures S4A and S4B) and in the absence of MHC-I/TCR inter-actions upon transfer of CD8⁺ T cells into *B2m*^{-/-} mice (Figures 4A and 4B). In addition,

calcineurin inhibitors FK506 or cyclosporin did not decrease CD8⁺ T cell expression of Tox, Tim3, and PD1 induced by anti-CD137 agonists (Figure 4C), whereas they decreased the percentage of memory CD8⁺ T cells from Ig control mice (Figure S4C). The use of fluorescent reporter Nur77^{GFP} transgenic mice⁶¹ in which T cells specifically express GFP in response to TCR stimulation confirmed that CD137-induced Tex cell expansion does not involve TCR stimulation. CD8⁺ T cells from Nur77^{GFP} mice did not express GFP in the different organs tested upon anti-CD137 treatment, in sharp contrast with anti-CD3+CD28 stimulation (Figures 4D, S4D, and S4E). Finally, we analyzed the single-cell TCR repertoire of sorted CD8⁺ Tmem, Tpex-like, and Tex-like treated with anti-CD137 or Ig control mAbs (see Figure 3G). We first calculated a clonal expansion score based on Shannon's entropy^{62,63} and compared it across transcriptional clusters and treatments. In both Ig and anti-CD137-treated animals, the highest TCR clonal expansion was found in the Tex-like cell subsets, specifically in clusters 3 and 4, respectively (Figure 4E). Yet, we observed a lower clonal expansion in the anti-CD137 condition, evidenced by the lower frequency of T cells belonging to large clones representing more than 1% of the total repertoire (Figures 4E and 4F). We next quantified the repertoire overlap between transcriptional clusters. In Ig control mice, Tpex-like cluster 1 and Tex-like clusters 3 and 4 were interconnected as shown by their high Morisita index⁶² (Figures 4G and 4H). Repertoire overlap between Tex clusters 3 and 4 was also evident upon anti-CD137-treatment, but these clusters were poorly connected with cluster 1 (Figures 4G and 4H). The lower clonal expansion and overlap of Tpex and Tex cells from CD137-stimulated mice are consistent with the TCR-independent Tex pathway induced by this receptor. To confirm these results, we wanted to compare common clonotypes found in Ig control and CD137 treated mice. If CD137 stimulation drives the expansion of existing Tex cells, we reasoned that the Tex cell TCR repertoire of anti-CD137-treated mice would include at least the TCR species found upon Ig treatment and potential additional clonotypes that were below detection in the Ig group. Because the mouse TCR repertoire is largely private, we did not quantify identical clonotypes, but rather TCR sequence-based groups using two different sequence-based methods (Levenshtein distance [LD] and Kidera factor [KF]).⁶² To avoid biases due to TCR groups containing few highly expanded TCRs, we only retained TCR groups of at least 100 cells and at least 10 clonotypes, which for the LD method only retained TCR alpha chain groups (Figure S4F). With both methods we observed that, while TCR groups derived from Tmem cells were equally likely to include cells from either condition, the Tpex and Tex subsets contained more TCR groups highly skewed for anti-CD137 treatment (Figures S4G and S4H). Collectively, these data indicate that, starting from the Tpex stage, CD137 agonism pushes toward exhaustion a similar repertoire to the one naturally found in naive mice, but also a broader number of TCR species, resulting in an overall more polyclonal repertoire.

T cell-intrinsic CD137-induced canonical NF- κ B signaling drives T cell exhaustion

To confirm that direct CD137 signaling accounts for the exhaustion program observed upon anti-CD137 treatment, we used *Cd137*^{-/-}(tomato⁺) and *Cd137*^{+/+}(tomato⁻) mixed BM chimeras (Figure 5A). Anti-CD137 mAbs induced the expansion of *Cd137*^{+/+} CD8⁺ Tmem cells with an exhausted phenotype while *Cd137*^{-/-} counterparts did not expand nor express exhaustion markers (Figures 5B–5D). Similar results were obtained when we transferred *Cd137*^{-/-} CD8⁺ T cells (CD45.2⁺) into *Cd45.1* mice (Figures S5A–S5C) or when *Cd137*^{+/+}

(tomato⁻) and *Cd137*^{-/-}(tomato⁺) CD8⁺ T cells were transferred into *Rag2*^{-/-}*Il2rg*^{-/-} mice (Figures S5D–S5F). In the latter model, we confirmed that anti-CD137 promoted the functional exhaustion of *Cd137*^{+/+} CD8⁺ T cell while *Cd137*^{-/-} CD8⁺ T cells were not affected (Figure S5G). Anti-CD137 treatment also increased the percentage of CD8⁺ Tex cells in the absence of other potential exhaustion-inducing inflammatory mediators^{19,64} as observed in *Ccl5*^{-/-}, *Il1r*^{-/-}, *Il6*^{-/-}, *Il10*^{-/-}, *Il12p40*^{-/-}, *Il18*^{-/-}, *Il27ra*^{-/-}, *Ifnar*^{-/-}, *Ifngr*^{-/-}, and *Tnf*^{-/-} mice (Figure S5H). Taken together, these results exclude the role of inflammatory mediators and demonstrate the intrinsic role of CD137 signaling in promoting CD8⁺ Tex cell expansion.

CD137 signaling relies on TNFR-associated-factor (TRAF) adapter proteins and more specifically TRAF1, TRAF2, and TRAF3.⁶⁵ CD8⁺ Tex cells expanded similarly in WT and *Traf1*^{-/-} mice upon treatment with anti-CD137 agonists (Figure 5E), thus suggesting a TRAF1-independent mechanism for CD137-induced T cell exhaustion. TRAF2 stimulates the canonical pathway involving NF- κ B heterodimers containing primarily p65 or cRel (encoded by *Rela* and *Rel* respectively) bound to p50, whereas TRAF3 promotes the non-canonical NF- κ B pathway consisting of RelB and p52 dimers (encoded by *Relb* and *Nfkb2* respectively).⁶⁵ Therefore to refine the CD137 signaling pathway promoting CD8⁺ T cell exhaustion, we explored the specific roles of the canonical and non-canonical NF- κ B subunits using *Cd4*^{cre} crossed with *Rela*^{fl/fl}, *Rel*^{fl/fl}, *Relb*^{fl/fl}, or *Nfkb2*^{fl/fl} mice.^{66–68} All of these different strains of mice underwent similar increase in CD44^{hi}CD62L⁻ CD8⁺ Tem cell upon anti-CD137 treatment (Figures 5F and 5G). In contrast, we observed a lower frequency of PD1⁺Tim3⁺ Tex cells in *Cd4*^{cre}*Rela*^{fl/fl} and *Cd4*^{cre}*Rel*^{fl/fl} compared with *Cd4*^{cre}*Relb*^{fl/fl}, *Cd4*^{cre}*Nfkb2*^{fl/fl}, and *Cd4*^{cre} control mice treated with anti-CD137 mAbs (Figures 5F, 5G, and S5J). While the levels of Tim3, PD1, and Eomes were reduced on CD8⁺ Tem cells from both *Cd4*^{cre}*Rela*^{fl/fl} and *Cd4*^{cre}*Rel*^{fl/fl}, only cRel deficiency significantly affected Tox expression (Figure S5I). The importance of canonical NF- κ B signaling in the Tex-inducing effects of CD137 was confirmed in our scRNA-seq datasets. In both tumor and non-tumor contexts, the NF- κ B signature was increased in the CD137 expanded Tex subsets (Figures 5H–5K). Conversely, we found that NF- κ B signature was decreased in *Cd137*^{-/-} CD8⁺ TILs compared with WT counterparts in mixed BM chimera bearing B16K1 tumors (Figure 5L). Taken together, these results confirm the importance of the canonical NF- κ B pathway and more particularly the RelA and cRel subunits in the CD8⁺ exhaustion program promoted by CD137 stimulation. Agonist antibodies directed against other TNFR receptors including GITR and OX40, that share signaling with CD137, did not promote the accumulation of CD8⁺ Tem cells with an exhausted phenotype when injected into WT mice suggesting that the NF- κ B-dependent stimulation of T cell is a specific feature of CD137 engagement by agonist antibodies (Figure S5J).

Anti-CD137 drives early epigenetic remodeling of Tex-cell-associated genes

The progressive epigenetic remodeling of CD8⁺ Tex-cell-associated genes such as inhibitory receptors is critical to enforce Tex cell program. To better understand the mechanism of the CD137-induced exhaustion program, we analyzed the splenic CD44^{hi} CD8⁺ T cell chromatin states along anti-CD137 treatment through assay for transposase-accessible chromatin using sequencing (ATAC-seq). Analysis of day 5 and day 18 anti-CD137 vs.

Ig differentially accessible peaks revealed that CD137 agonism induces early chromatin remodeling that is strengthened in the course of treatment (Figures 6A, S6A, and S6B). Among the 10,101 open peaks after 18 days of CD137 stimulation, 3,602 were already opened at day 5 ($\log_2\text{FC} > 2$ adjusted [adj] $p < 0.01$) (Figures 6B and 6C). These were enriched in LCMV and tumor exhaustion signature genes, indicating that CD137 engagement rapidly promoted CD8⁺ T cell exhaustion program at the chromatin level (Figures 6D and 6E). Increased ATAC signals were clearly visible in the promoter and regulatory regions of exhausted signature genes such as *Pdcd1*, *Havcr2*, *Lag3*, *Gzmk*, *Nr4a2*, and *Tox* after anti-CD137 treatment (Figures 6F, S6C, and S6D). These included two Tex cells' selectively accessible open chromatin region located at -22 kb 5' of the *Pdcd1* TSS and ~ 3 kb 3' of the *Lag3* gene.^{4,69,70} We next performed TF inference for differentially accessible peaks between Ig and CD137 condition using chromVAR package⁷¹ that confirmed the importance of NF- κ B canonical pathway in the epigenetic changes induced by anti-CD137 treatment. Indeed, CD137 differentially accessible peaks were enriched in NF- κ B pathway especially at D5 and promoters differentially opened by CD137 were enriched NF- κ B canonical pathway (Figures 6G, S6E, and S6F). Together these data confirm that NF- κ B-dependent CD137 signaling directly regulates the T cell exhaustion program at the epigenetic level.

Tox has been shown to play a critical role in the chromatin remodeling of Tex-specific genes.^{11,12,14,15} Tox expression was decreased in *Cd137*^{-/-} CD8⁺ TILs compared with WT counterparts in mixed BM chimeras bearing B16K1 tumors (Figure 6I). Conversely, CD137 agonists induced Tox expression by CD8⁺ T cell in a cRel-dependent manner (see Figure S5I), suggesting a link between CD137 signaling, Tox, and Tex cell program. To address this hypothesis, we generated CD45.1 CRISPR-Cas9 control and CD45.2 CRISPR-Cas9 Tox-deficient CD8⁺ T cells by nucleofection of sgRNA plus Cas9 protein RNPs, which were co-transferred into *Rag2*^{-/-} *Il2rg*^{-/-} mice (Figure 6J). CD45.1 control CD8⁺ T cells had increased expression of Tox, PD1, Tim3, and LAG3 upon treatment with anti-CD137 while CD45.2 Tox-deficient CD8⁺ T cells failed to up-regulate these markers (Figure 6K). Thus, our data point toward a role for Tox-induced epigenetic remodeling in CD137-induced T cell exhaustion.

Contrasting effect of anti-CD137 on immune surveillance and anti-PD1 efficacy

Finally, we wanted to determine whether Tex cell accumulation induced by systemic anti-CD137 treatment may affect anti-tumor immunosurveillance *in vivo*. To address this point, WT mice were pre-treated with anti-CD137 mAbs for 3 weeks, before being challenged with B16K1 (Figure 7A). Anti-CD137 pre-treatment increased tumor burden compared with Ig control (Figure 7B). These results were confirmed in the B16F10 and VK12653 models (Figures S7A–S7C). A short anti-CD137 conditioning of 4 days before B16K1 injection was sufficient to increase tumor growth compared with Ig control, confirming that anti-CD137-induced Tex cell expansion may limit anti-tumor efficacy (Figure 7A). Adoptive transfer of PD1⁺ Tex or PD1⁻ Tmem cells from OT-1 mice treated with anti-CD137 mAbs into *Rag2*^{-/-} *Il2rg*^{-/-} mice injected with B16-ova confirmed that Tex cells expanded upon anti-CD137 treatment have lower anti-tumor functions than their Tmem counterparts (Figures 7C and 7D). Anti-PD1 treatment only partially reversed dysfunctions induced by anti-CD137

treatment (Figure S7D). Indeed, anti-PD1 treatment decreased tumor growth in anti-CD137 pre-treated mice although anti-PD1 efficacy was still reduced compared with anti-PD1 treatment alone (Figure S7D). Accumulating evidence supports that activation of T_{pe}x cells in the DLN, rather than TermTex cell reinvigoration, is a key mechanism underlying anti-PD1 efficacy.^{23,50,72} Given the ability of CD137 stimulation to drive the expansion of CD8⁺ T_{pe}x cells, we reasoned that anti-CD137 agonists may have better efficacy when injected after anti-PD1 mAbs. To address this, WT mice with detectable B16K1 or B16-ova tumors were treated with either anti-PD1, anti-CD137, or a combination of both mAbs (Figure 7E). Anti-PD1 treatment on well-established tumors (day 9) limited tumor progression but was not sufficient to promote tumor regressions (Figures 7F and 7G). Again, anti-CD137 was poorly effective in reducing tumor growth when injected on well-established tumors consistent with previous report.⁷³ In contrast, anti-CD137 treatment given after anti-PD1 decreased tumor burden and prolonged survival compared with anti-PD1 in both B16-ova model and B16K1 models (Figures 7F and 7G). Of note, anti-PD1 limited tumor progression in both *Cd137*^{-/-} and *Cd137*^{+/+} mice (Figures S7E–S7G). While we have not ruled out that the accumulation of T_{pe}x cells triggered by the systemic CD137 agonist injection may favor tumor relapse and limit subsequent immunotherapeutic interventions, the combination of anti-PD1 followed by anti-CD137 provides a clear enhancement of tumor rejection in the models we have examined.

DISCUSSION

CD137 is an intriguing receptor with potential therapeutic applications, as a target of agonist agents, in both cancer and autoimmune disease. Thus, there is a clear need to understand the functional ramifications of CD137 signaling. Here, through transcriptomic, epigenomic, and functional assays, we demonstrated the importance of T cell-specific CD137 signaling in CD8⁺ T cell exhaustion program. Using T cell-specific CD137-deficient mice, we found that CD137 absence limited tumor associated T_{pe}x cell in different mouse tumor models. CD137 was specifically expressed by CD8⁺ T_{pe}x cells and CD137 agonists promoted the TCR-independent, NF- κ B-dependent proliferation and terminal differentiation of these cells. Finally, while T_{pe}x cell accumulation induced by prophylactic anti-CD137 treatment favored tumor escape, we found that PD1 efficacy is improved with subsequent CD137 stimulation.

We have provided extensive evidence that T cell-intrinsic CD137 signaling is an important component favoring T_{pe}x cell expansion and differentiation, thus raising questions about the role of TCR signaling in this mechanism. Chronic TCR stimulation represents the main, if not the only known, driver of CD8⁺ T cell exhaustion.^{8,13,74} Yet, experiments with Nur77^{GFP} TCR reporter, TCR transgenic MHC-I-deficient mice, or calcineurin inhibitors all point toward a TCR/calcineurin-independent T_{pe}x-cell-promoting role of CD137. In contrast, our results revealed the importance of RelA and cRel subunits in the T_{pe}x-cell-inducing effects of CD137, suggesting that the activation of canonical NF- κ B pathway may favor CD8⁺ T_{pe}x cell program. Our findings raise the question whether additional TNFR members that share signaling pathways with CD137 may also promote T cell exhaustion program. However, neither OX-40 nor GITR agonists induced exhaustion-associated markers in our experiments, even though both receptors promote TRAF2-dependent NF- κ B signaling and

survival like CD137.⁷⁵ Future experiments are required to refine the CD137 signaling that stimulates Tex cell expansion.

Our results do not exclude the role of TCR signaling in T cell exhaustion. Indeed, we found that CD137 stimulation did not affect naive or PD1⁻ memory CD8⁺ T cells and rather expanded and promoted the terminal differentiation of cells already committed to a Tex-like program. Indeed, flow cytometry and scRNA-seq analysis, in human and mouse tumoral and chronic infected tissues, all support the CD8⁺ T cell-specific expression of CD137 by Tex cells. Notably, the analysis of public datasets^{10,41,52} showed that *Tnfrsf9* expression is restricted to Tex cell populations that arise upon chronic LCMV or tumors but not *bona-fide* effector memory CD8⁺ T cells found in acute LCMV infections. While chronic TCR signaling may account for CD137 expression by Tex cells, several TCR-independent mechanisms were identified, including IL-15 or IL-2⁷⁶ and GITR-induced expression.⁷⁷ Hypoxia driven Hif1 α also induces CD137 expression in the tumor context.⁷⁸ TCR-independent expression of CD137 was suggested to contribute to the maintenance of a CD8 Tmem cell pool in the absence of their specific antigen.⁷⁶ Our results suggest a similar mechanism whereby high CD137 expression on CD8⁺ Tex cells may contribute to their maintenance and expansion even in the absence of active TCR signaling.

Many laboratories, including ours, have found an anti-tumor function of anti-CD137 agonists against diverse tumor models.^{31,33,35} Yet, despite promising pre-clinical results, the clinical efficacy of anti-CD137 mAbs was limited in the different clinical trials that also revealed severe adverse events (SAEs) in the case of the human anti-CD137 mAb urelumab.^{34,35} The systemic expansion of Tex cells with limited effector functions induced by anti-CD137 mAbs may account for the so-far disappointing efficacy of CD137 agonists. Indeed, we found that the prophylactic treatment of mice with anti-CD137 mAbs subsequently increased the growth of different immunogenic tumor models and limited the efficacy of anti-PD1 immunotherapy. In line with these results, anti-CD137 agonists have been shown to limit autoimmune disease in several mouse models.³⁶⁻³⁹ The systemic expansion of Tex cells may also account for the SAE induced by anti-CD137 in cancer patients.^{34,35} Indeed, aged patients have a long history of infections and may contain a larger repertoire of CD8⁺ Tex cells that could expand and may be responsible for liver inflammation upon systemic CD137 stimulation.⁷⁹⁻⁸¹ These results highlight the importance of therapeutic strategies favoring intratumor delivery of anti-CD137 mAbs to limit the risk of systemic activation of bystander Tex subsets, although the long-term benefit for TILs is still hypothetical.^{82,83}

The T cell exhaustion program is often considered as a tumor escape mechanism limiting anti-tumor functions of CD8⁺ T cells.⁵ Indeed, Tex cells have reduced effector functions and display high levels of inhibitory receptors. Yet Tex cells are not inert, and T cell exhaustion may not always be unfavorable in cancer and chronic infectious disease.¹⁶ Indeed, Tex cells present residual functions, which may be important *in vivo* for control of tumor growth and viral replication. For example, depletion of CD8⁺ Tex cells during the chronic phase of simian immunodeficiency virus (SIV) infection resulted in exacerbation of viremia.⁸⁴ Here, we found that decreased Tex cell frequency in CD137-deficient mice reduced CD8⁺ T cell infiltration and increased tumor growth as compared with WT counterparts. Similar decrease

in effector T cell persistence was described in chronic infectious disease in the absence of Tox.¹³ Thus, the Tex cell program seems to ensure chronic pathogen or tumor control while limiting T cell-mediated immunopathology that fully activated cells would engender. Manipulating such subsets represents one of the most promising anti-tumor strategies. Yet, pre-existing tumor-specific T cells may have limited reinvigoration capacity, and the T cell response to checkpoint blockade rather derives from a distinct repertoire of T cell clones that may have recently entered the tumor.⁸⁵ In this context, Tex cell expansion by anti-CD137 agonists may be useful and could improve ICB efficacy, as shown in our tumor mouse models.

Limitations of the study

We found that the impact of CD137 deficiency on Tpex cells was more modest than on TermTex cells in the mixed chimera tumor model. This suggests that Tpex cells, at least in tumors, may depend less on CD137 than TermTex cells although CD137 stimulation by agonists quickly promoted Tpex cell proliferation. These questions regarding the relative importance of CD137 in the different Tex cell subset remains to be addressed. In addition, further experiments are required to determine the source of CD137-L in the tumor context. While activated DCs express high level of CD137-L, they might not be the only source in tumor contexts as many tumor cell types have been shown to express this ligand.⁸⁶ Finally, the importance of CD137 signaling for Tex expansion differentiation or persistence in chronic infectious disease will need to be investigated.

STAR★METHODS

RESOURCE AVAILABILITY

Lead contact—Further information and requests for resources and reagents should be directed to and will be fulfilled by the lead contact, Ludovic Martinet (ludovic.martinet@inserm.fr).

Materials availability—Unique reagents and cell lines generated in this study may be made available on request (pending continued availability) from the lead contact with a completed materials transfer agreement.

Data and code availability—The datasets in this publication have been deposited in NCBI's Gene Expression Omnibus and are accessible through GEO Series accession numbers GSE205702, GSE205703, GSE230626, and GSE228271. All analyses were done with custom R scripts and are available upon request using standard R packages. No new algorithms were developed during this study.

EXPERIMENTAL MODEL AND STUDY PARTICIPANT DETAILS

Mouse models—Mouse strains were maintained either in the SPF animal facility of the US006 CREFRE-Inserm/UPS which is accredited by the French Ministry of Agriculture (accreditation number A-31 55508). Unless specified tumor experiments used both male and female mice between 6 and 12 weeks of age. Donors and recipients of adoptive T cell transfers were sex matched. Animal experiments were conducted and approved by the Ministère de l'Enseignement Supérieur, de la Recherche et de l'Innovation (APAFIS#5614–

20 16060815487810 v4) and are in compliance with the French regulations on care and protection of laboratory animals. For survival analysis, mice were monitored daily according to institutional ethic guidelines, and were euthanized when mice developed signs of reduced mobility including paralysis, hunched posture, or respiratory distress. All mice used in this study were on a C57BL/6 genetic background. WT mice were purchased from Janvier laboratories. *Ifngr*^{-/-}, *Ifnar*^{-/-}, *Il12p40*^{-/-}, *Il18*^{-/-}, *Il6*^{-/-}, *Tnf*^{-/-}, *Il10*^{-/-}, *Il1r*^{-/-}, *Il27ra*^{-/-}, *Ccl5*^{-/-}, *Rag2*^{-/-} *Il2rg*^{-/-}, *B2m*^{-/-}, *OT1* and *CD45.1* mice have already been described. *ROSA26^{tomato}xCd137^{fl/fl}* and *Cd137^{fl/fl}* mice were generated by Dr. B. Salomon (Infinity, Toulouse) and crossed with *Cd4^{cre}* mice. *Cd4^{cre}* crossed with *Rela^{fl/fl}*, *Rel^{fl/fl}*, *Relb^{fl/fl}* or *Nfkb2^{fl/fl}* mice were kindly provided by Dr Yenkel Grinberg-bleyer (CRCL, Lyon). *Traf1*^{-/-} mice were kindly provided by Dr T. Watts (University of Toronto).

Cell lines and cell culture—B16F10 melanoma cell line and variants stably expressing the MHC-I molecule H-2Kb (B16K1)⁸⁷ or ova (B16-ova) as well as MC38 colon cancer cell line were used in this study. B16F10, B16-ova and B16K1 cells lines were cultured in DMEM medium containing 10% heat-inactivated fetal calf serum (FCS); MC38 were cultured in DMEM medium High glucose containing 10% heat-inactivated fetal calf serum (FCS). Cells were tested negatively for mycoplasma contamination and maintained in culture for a limited number of passages. Transplantable Vk*MYC MM cell line (Vk12653) was kindly provided by Bergsagel. L (Mayo clinic, USA). Transplantable MM cell line Vk12653 were generated and expanded as previously described.^{33,96}

METHOD DETAILS

Flow cytometry—Single cell suspensions were stained according to standard protocols with previously described anti-mouse and human antibodies listed in the key resources table. Antibodies were purchased from miltenyi biotec, eBioScience, BioLegend, or BD Biosciences. Surface staining was performed with Abs for 30 min at 4 °C in PBS supplemented with 2% FCS and 2 mM EDTA. For the intracellular staining, cells were fixed and permeabilized using BD Cytotfix/Cytoperm permeabilization kit (BD Biosciences) or Transcription Factor Fixation/Permeabilization kit (Thermofisher).

Mouse tumor implantation, tumor measurement, and tumor digestion—The left flank of mice was shaved and B16F10 (5.10⁵), B16K1 cells (10⁶), B16-ova cells (10⁶), MC38 cells (2.10⁶) were injected subcutaneously (s.c.) in 100 µl of PBS. Tumor area and volume were estimated by measuring the tumor size in two dimensions using a caliper. Tumors were measured three times per week. Mice were sacrificed at the indicated time points or when the estimated tumor volume reached 2 cm³. TILs were analyzed as previously described. Briefly, solid tumors were excised, manually dissociated and enzymatically digested with Tumor Dissociation Kit (Miltenyi Biotec) and then incubated at 37 °C for 30 min. After incubation, digested tumors were mashed through 70µm filters and immune cells were enriched using CD45 microbeads (Miltenyi Biotec) before TILs analysis. Vk12653 MM cells (2.10⁶) were injected i.v. into tail vein of indicated strains of mice. The percentage of monoclonal Ig in the serum was quantified by serum protein electrophoresis (Sebia Hydrasys system). The phenotype, percentage and number of BM

B220⁻ CD138⁺CD155⁺PCs and CD8⁺ TILs were analyzed by flow cytometry at the indicated time points as described previously.³³

Mouse T-cell functional assays—For cytokine production assays, freshly isolated CD8⁺ Tem cells or PD1⁺ and PD1⁻ CD8⁺ T cells were isolated using mouse CD8⁺ T cell isolation kit (Miltenyi Biotec) and FACSaria™ Fusion (BD biosciences) and were stimulated with plate-bound anti-CD3 (0.3–3 µg/ml, 145–2C11, Biolegend) and soluble anti-CD28 (1 µg/ml, 37.51, Biolegend) or with Phorbol myristate acetate (PMA; 50 ng/ml, Sigma) and ionomycin (1 µg/ml, Sigma) in the presence of Golgi Plug (BD biosciences) for 5 h. Intracellular cytokine staining was performed as described above. For T cell proliferation assay, freshly sorted CD8⁺ T cells were loaded with CTV (Thermo Fisher Scientific) according to manufacturer's instructions prior to stimulation. CTV dilution was analyzed after 4 days. Cytokine levels were measured in the corresponding cell culture supernatants by Cytometric Bead Array (CBA, BD Biosciences) after 48 hrs.

CD8⁺ T cell gene editing—Ribonucleoprotein (RNP) complexes were assembled using recombinant Cas9 (IDT) and predesigned Alt-R CRISPR-Cas9 gRNAs (IDT) duplexed with atto550 conjugated tracrRNA (IDT). CD8⁺ T cells were isolated from the spleen as previously described and 10⁶ CD8⁺ T cells were resuspended in 20µL P3 primary cell nucleofection buffer (Lonza), mixed with 5µL of Cas9-RNP complex and transferred to wells of a 16 well nucleocuvette strip (Lonza-V4XP-3032). CD8⁺ T cells underwent nucleofection using the DN100 program in a Lonza 4D-nucleofector device. Immediately after nucleofection, cells were harvested and cultured in complete RPMI supplemented with IL-7 (10 ng/mL) for 24 hrs. Following incubation, cells were harvested and washed. 10⁶ CD8⁺ T cells were adoptively transferred into recipient mice. For negative control treated cells, RNP complexes included negative control crRNA #1 (IDT). For *tox* targeted cells, RNP complexes included three predesigned sgRNAs (IDT) targeting the *tox* gene. Guides: Mm.Cas9.TOX.AA – AACCGGATTCTACCTCATTC; Mm.Cas9.TOX.AB – GATCACGGTGTCCAACATGC; Mm.Cas9.TOX.AC – TTTGTTCTTTTCGTGATACCC Negative control scrRNA #1 – cat# 1072544 (IDT) – no guide sequence publicly available.

TNFR agonist treatment—C57BL/6 WT were treated by i.p. injection of anti-CD137 (1–100 µg, mIgG2a 3H3 or mIgG1 Lob12.3, BioXcell, twice a week), anti-OX40 (200 µg; OX-86, BioXcell, twice a week), anti-GITR (200µg; DTA-1, BioXcell, twice a week) or with control IgG mAbs (HRPN, BioXcell). After 2–3 weeks, lymphoid organs were isolated for CD8⁺ T cell phenotypic analysis and functional assays.

CD137 prophylactic treatment—Groups of C57BL/6 wild type (WT) were conditioned with anti-CD137 (10 µg, mIgG2a 3H3, BioXcell, twice a week) or IgG mAbs (HRPN, BioXcell) for the indicated period and subsequently injected s.c. with B16K1, B16F10 or VK12653 cells. In some B16K1 experiments mice were treated with anti-PD1 (200 µg i.p., RMP1–14 on days 6, 9, 12 relative to tumor inoculation) or with cIg (200 µg i.p.; 2A3, BioXCell).

Immune checkpoint blockade combination—The indicated group of mice bearing palpable B16-ova, B16K1 or MC38 tumors (25–50 mm² area) were treated with anti-PD1

(200–250 µg i.p., RMP1–14, 3 shots on day 9, 12, 15 relative to tumor inoculation) or with cIg (200 µg i.p.; 2A3, BioXCell). Ig or anti-PD1 treated mice were treated with anti-CD137 (10 µg, mIgG2a 3H3, BioXcell, on day 15, 18, 21 relative to tumor inoculation) or IgG (HRPN, BioXcell).

Cell transfer experiments—For Figure 2D, 1.10^7 OT-1 splenocytes were injected i.v. into *Cd45.1* mice that were subsequently injected with B16-ova on day 1. Mice were treated with anti-CD137 (10 µg, mIgG2a 3H3, BioXcell, on day 7, 11, 14, 17) or IgG (HRPN, BioXcell) and sacrificed on D21 for CD45.2⁺ OT-1 TIL FACS analysis. For Figures S4A and S4B, 3.10^7 OT-1 splenocytes were injected i.v. into WT mice that were subsequently treated with anti-CD137 (10 µg, mIgG2a 3H3, BioXcell, twice a week) or IgG control. For Figure 7C, OT-1 mice were treated 18 days with anti-CD137 mAbs (100 µg, mIgG2a 3H3, BioXcell twice a week) and 5.10^5 FACS sorted splenic PD1⁻ Tmem or PD1⁺ Tex cells were transferred into *Rag2^{-/-}Il2rg^{-/-}* mice. After 6 days mice were injected with B16-ova cells and monitored for tumor growth and survival. For Figures 4A and 4B, 3.10^6 CD8⁺ T cells isolated from WT mice and were injected i.v. into *B2m^{-/-}* mice that were subsequently treated with anti-CD137 or Ig control. For Figures 3E and 3F, 5.10^5 Tn (CD44⁻ CD62L⁺), Tmem (PD1⁻ CD44^{hi}) and Tex cells (CD44^{hi} PD-1⁺) were FACS sorted from 15 weeks *Cd45.1* mice and were injected i.v. into *Cd4^{cre}Cd137^{fl/fl}* mice that were treated with anti-CD137 mAbs (3H3, 10 µg) or IgG control. For Figures 3L–3N, S1E, S1F, and S5D–S5F, *Rag2^{-/-}Il2rg^{-/-}* mice were injected with 5.10^5 splenocytes, isolated from *Cd4^{cre}Cd137^{fl/fl}ROSA26^{tomato}* (CD137^{-/-}tomato⁺) and *Cd137^{fl/fl}ROSA26^{tomato}* (CD137^{+/+}tomato⁻) littermates, or with 5.10^5 PD1⁻ (Tmem), PD1⁺SLAMF6⁺Tim3⁻ (Tpex-like) or PD1⁺SLAMF6⁻Tim3⁺ (Tex-like) splenic CD44^{hi}CD8⁺ T cells isolated from WT mice. For Figures 6J and 6K 10^6 nucleofected Tox KO CD45.2 and ctrl CD45.1 CD8⁺ T cells were adoptively transferred into *Rag2^{-/-}gC^{-/-}* mice by tail vein injection. After one week, mice were treated with anti-CD137 mAbs (clone 3H3, BioXcell) on day 7, 11, 15 and 18. At D21, mice were euthanized, spleen collected and transferred cells were analyzed by flow cytometry as mentioned above.

Hematopoietic chimeras—C57BL/6 mice were lethally irradiated (9 Gray) and reconstituted by intravenous injection of 5.10^6 BM cells from *Cd4^{cre}Cd137^{fl/fl}ROSA26^{tomato}* and *Cd137^{fl/fl}ROSA26^{tomato}* or *Cd4^{cre}Cd137^{fl/fl}* and *Cd45.1*. The reconstitution of the immune system of the recipient mice was verified 7 weeks after BM transplantation by blood analysis. Mice were subsequently treated with anti-CD137 or IgG control mAbs or injected with B16K1 cells or MC38 as described above.

Calcineurin inhibitor experiments—C57BL/6 WT were treated by i.p. injection with anti-CD137 (10 µg; 3H3, BioXcell, twice a week) or control IgG (HRPN, BioXcell), and were treated daily with FK506 (invivogen, i.p. injection 3 mg/kg) or with cyclosporine A (invivogen, oral gavage, 28 mg/kg). Mice were sacrificed at day 14, and CD8⁺ T cells from spleen were prepared for phenotypical analyses.

3' single-cell RNA-sequencing—C57BL/6 mice were injected with Vk12653 MM cells. After 10 days, mice were treated with anti-CD137 (100 µg, 3H3, BioXcell, twice

a week) or with control IgG (100 µg, HRPN, BioXcell). At the indicated time points, CD8⁺ T cells were isolated from the BM using mouse CD8⁺ T cell isolation kit (Miltenyi Biotec) and FACSaria™ Fusion (BD biosciences). Single-cell libraries (3' gene expression) were generated using the Chromium Controller Instrument and Chromium Single Cell 3' Library & Gel Bead Kit v3 according to the manufacturer's protocol (10× Genomics). Single-cell library size and quality were confirmed on the Fragment Analyzer (Agilent). KAPA Quantification Kit for Illumina platforms (KAPA Biosystems, Roche) was used to quantify libraries. The libraries were sequenced on a NextSeq 550 (Illumina) in pair-end sequencing 28 bp (read1) × 91 bp (read2) and a single index 8 bp in length.

5' single-cell RNA-sequencing—Tomato⁺ and tomato⁻ spleen and tumor CD8⁺ T cells were isolated from (CD137^{-/-} tomato⁺) and (CD137^{+/+}tomato⁻) mixed BM chimera bearing B16K1 for 19 days using FACSaria™ Fusion.

Single-cell libraries (5' gene expression) were generated using the Chromium Controller Instrument and Chromium Next GEM Single Cell 5' Library & Gel Bead Kit v1.1 according to the manufacturer's protocol (10X Genomics). Additional Chromium Single Cell V(D)J Enrichment Kit, Mouse T Cell were used to generate TCR Libraries. Single-cell library size and quality were confirmed on the TapeStation 4200 (Agilent) and pooled to reach at least 20,000 read pairs for 5' Gene Expression Library; 10,000 read pairs of Protein Library and 5,000 read pairs of V(D)J Library. Libraries were sequenced twice on a NextSeq 550 (Illumina) in pair-end sequencing 26 bp (read1) × 91 bp (read2) and a single index 8 bp in length. A similar workflow was performed on spleen memory CD8⁺ T cells (CD44^{hi}/PD1⁻), precursor exhausted T cells (CD44^{hi}/PD1⁺/Slamf6⁺/Tim3⁻), and exhausted T cells (CD44^{hi}/PD1⁺/Slamf6⁻/Tim3⁺) sorted using FACSaria™ Fusion from C57BL/6 mice treated with anti-CD137 (10 µg, 3H3, BioXcell, twice a week, 5 mice) or with control IgG (100 µg, HRPN, BioXcell, twice a week, 10 mice) for 14 days.

ATAC-seq sample preparation—C57BL/6 mice were treated with anti-CD137 (10 µg, 3H3, BioXcell, twice a week) or with control IgG (10 µg, HRPN, BioXcell). At the indicated time points, splenic CD44^{hi}CD8⁺ T cells were isolated using FACSaria™ Fusion (BD biosciences). ATAC-seq was performed as previously described.⁹⁷ Briefly, 50 000 cells were lysed in ice-cold lysis buffer and the transposition reaction was performed using the Tn5 transposase at 37 °C for 30 min. DNA was purified using the QIAGEN MinElute kit (QIAGEN). The libraries were prepared using the Nextera DNA Library Prep Kit (Illumina) and purified using AMPure XP beads (Beckman) following a double-sided protocol to remove primer dimers and large fragments. Samples were performed in duplicates, multiplexed and sequenced on NextSeq-500 (75 bp paired-end reads).

QUANTIFICATION AND STATISTICAL ANALYSIS

Statistical analyses were performed using GraphPad Prism 9 Software. Mann-Whitney U test or paired and unpaired student t test were used for single comparisons between two groups. For comparison of three or more groups, one-way ANOVA with Tukey's multiple comparison test, Holm-Sidak multiple test correction, or non-parametric Kruskal-Wallis test with Dunn's multiple comparison post-test were used. Differences in survival were evaluated

with the Mantel-Cox test. $P < 0.05$ was considered statistically significant ($P < 0.05 = *$; $P < 0.01 = **$; $P < 0.001 = ***$).

Flow cytometry—Data were collected with Aurora (Cytex Biosciences), LSR II or Fortessa X20 flow cytometers (BD Biosciences) and analyzed with FlowJo software (TreeStar). Dead cells and doublets were excluded by LiveDead staining (Thermo Fisher Scientific).

Single-cell RNA-seq analysis

Cell-level quality control, dimensionality reduction, and clustering: Raw data (FastQ files) for expression, antibody detection and V(D)J repertoire quantification were generated with CellRanger mkfastq and aligned and demultiplexed with CellRanger count or CellRanger vdj. For the anti-CD137 sorted subsets dataset, CellRanger count was rerun with the option `-force-cells` to correct for inconsistencies between the number of cells identified in the first round of alignment/demultiplexing and the number of cells calculated upon inspection of the barcode rank plot. For the anti-CD137 dataset and CD137^{-/-} dataset, data were then loaded in an R session with the Seurat 3.0 toolkit package involving the normalization and variance stabilization package `sctransform`.⁹⁸ For the anti-CD137 sorted subsets dataset, data were log-normalized. Samples were individually filtered using the following criteria: for the anti-CD137 and CD137^{-/-} dataset, we kept cells with 30,000UMIs and < 25% mitochondrial genes. For the anti-CD137 sorted subsets dataset, we retained cells with a number of unique RNA features between 500 and 4000 and less than 10% of mitochondrial genes. For the anti-CD137 sorted subsets dataset, cells were scored by for the cell cycle phase using genes from this source (https://github.com/hbc/tinyatlas/blob/master/cell_cycle/Mus_musculus.csv) as input. The cell cycle score was then regressed during data scaling to generate inputs for principal component analysis. Using Seurat, data sets were reduced by PCA, using the first 13 (anti-CD137 dataset) and 10 (CD137^{-/-} dataset, anti-CD137 sorted subsets dataset) principal components to reduce dimensionality by Uniform Manifold Approximation and Projection (UMAP). A resolution parameter set the granularity at 1.2 for the clustering by the K-nearest neighbor graph-based clustering approach of Seurat's Find Clusters function.

Signature scores—In Figures 1J and S2D, signature scores were computed with Single-Cell Signature Explorer Scorer⁹⁹ with signatures downloaded from MsigDB¹⁰⁰ or using published signatures.^{19,40,41,49} In all the other figures, signature scores were calculated using the `AddModuleScore` function of Seurat. The mouse `nfkB` signature was obtained at this address (<https://bioinfo.lifl.fr/NF-KB/>) and has been curated and maintained by the Gilmore Lab at Boston University. All the other mouse signatures were obtained from lists of genes found differentially expressed between indicated conditions of interest that were provided in supplementary tables in the relative publications. After subsetting these lists to include only genes that were upregulated with an adjusted p value smaller than 0.05, they were provided as input to the `AddModuleScore` function.

Relative likelihood estimate using MELD—MELD¹⁰¹ was run on the PCA cell embedding matrix, with the genotype of the cell as the raw experimental signal.

Single-cell reference mapping—The anti-CD137 dataset was projected on a reference dataset of exhausted T cells⁵² using the Seurat functions FindTransferAnchors, TransferData, MapQuery as described at this address (https://satijalab.org/seurat/articles/integration_mapping.html)

TcR clonal expansion analysis—TcR repertoire analyses were performed using the R package scRepertoire.⁶² To match clonotypes and single cell transcriptomes, and classify cells into clonal expansion bins, we used the function combineExpression() with the argument “proportion” set as TRUE. The clonal expansion score was calculated with the scRepertoire function StartracDiversity(), which incorporates the STARTRAC software.⁶³ In order to take into account the confounding effects of sample size on clonal expansion estimates, for the data presented in Figure 4F we generated a list of 10 randomly sampled subsets of the original data. The size of these replica downsamples was set at 90% of the smallest sample between the Ig and anti-CD137 condition, for each of the three subsets.

TcR clonal overlap analysis—To measure the TcR overlap between Tpex and Tex clusters, we calculated the Morisita index, for either treatment separately, using the scRepertoire function clonalOverlap(method = “morisita”). To visualize the TcR overlap, we generated circos plots with the scRepertoire function getCirclize() and the circlize function chordDiagram().

TcR sequence-based groups analysis—To group TcRs into sequence-based similarity groups, we used the scRepertoire function clusterTCR() with the value “aa” to the argument “sequence”, as well as the function runTrex() from the Trex package (<https://github.com/ncborcherding/Trex>) with the value “KF” to the argument “AA.properties”. The outputs of RunTrex was used as input for the Seurat functions RunUMAP(), FindNeighbors() and FindClusters(). TcR group membership was then used to calculate a treatment skew, by computing the percentage of cells in each TcR group that were derived from Ig-treated or aCD137-treated mice. Statistical significance of this skew was determined by computing the Pearson’s Chi-squared test with Yates’ continuity correction with the R package stats.

ATAC seq bioinformatic analysis—trimGalore (v0.6.5) (<https://github.com/FelixKrueger/TrimGalore>) was used to remove adapters and low-quality ends (Phred score<20). Reads smaller than 20 bp were also discarded. After read trimming, FastQC (v0.11.7) (<https://github.com/s-andrews/FastQC>) were performed to check the successful removal of adapter and low-quality bases. Trimmed reads were then mapped to the new murine reference genome (GRCm39) using STAR (v2.6.0c)⁹¹ aligner with “alignIntronMax” parameter set to 1 turning off splicing. Multiple and duplicated reads were removed with samtools (v1.9) (<https://github.com/samtools/samtools>) and MarkDuplicates of Picard package (v1.88) (<https://github.com/broadinstitute/picard>) respectively. Enriched peaks were called using MAC2 (v2.1.0.20150731) (<https://github.com/macs3-project/MACS>) with default parameters. BigWig files were generated with bamCoverage function of deeptools (v3.3.1) (<https://github.com/deeptools/deepTools>) package and were normalized with quantile function of ChIPin package (v0.1.0).⁹⁴

Identification of differentially accessible regions (DAR)—To identify differentially accessible regions, we merged the peaks detected by MAC2 (v2.1.0.20150731) in all conditions with bedtools merge function (v2.27.1) (<https://github.com/arq5x/bedtools2>). The signal on peaks was quantified with get_coverage function of megadepth package (1.8.0) (<https://github.com/LieberInstitute/megadepth>). The differential analysis was performed in pairwise (CD137 J18 vs Ig / CD137 J5 vs Ig) with DESeq2 (v1.38.3).⁹⁵ The peaks were defined as differentially accessible if their absolute value of log₂ fold change is greater than 2 and p-value adjusted lower than 0.01. ATAC signals around up and down DARs (−1.5Kb +1.5 Kb) for each sample were visualized using computeMatrix and plotHeatmap functions of deeptools tool (v3.5.1) (<https://github.com/deeptools>). The genomic tracks were generated using pyGenomeTracks (v3.8).¹⁰² The peak annotation of DAR was realized using annotatePeaks.pl function of the HOMER package (v4.10.4) (<https://github.com/IGBIllinois/HOMER>).

Identification of differentially accessible promoters and ingenuity pathways analysis (IPA)—The promoters were defined as the regions surrounding ±2Kb the TSSs of the genes. The differential analysis was performed as explained above for the identification of differential accessible regions. The fold changes and pvalues calculated by DESeq2 were processed by IPA tool¹⁰³ to determine likely upstream regulators using machine learning methods. The most significant regulators predicted in the analysis are summarized in a graphical summary network.

Transcription factor inferring—To identify transcription factors potentially responsible for the differential ATAC signal observed downstream of treatment with anti-CD137, we first downloaded motifs from the JASPAR database (v0.99.10)¹⁰⁴ using the function getJasparMotifs of chromVar package (v1.20.2) (<https://github.com/GreenleafLab/chromVAR>). Then, we realized the motif enrichment analysis using the function matchMotifs from the motifmatchr package (v1.20.0) (<https://github.com/GreenleafLab/motifmatchr>) using GRCm39 as a reference genome. To compute accessibility deviations for each motif in each condition, we used computeDeviations function from chromVar package (v1.20.2), that calculates the difference between the total number of reads mapping to peaks containing a given motif relative to an expected number of reads. Finally, we called computeVariability function of chromVar to get: 1/variability, that represents the standard deviation of the scores computed above and thus estimates the degree of involvement of the associated transcription factor in explaining the differences observed, and 2/ pvalue for the variability calculated being statistically significant.

Human scRNA-seq data—For the melanoma dataset,⁴⁷ gene expression matrices and metadata were obtained from dbGaP (accession number phs002289.v1.p1) and normalization, cell-level QC and dimensionality reduction were performed as described in the original publication. For clarity purposes, the original clusters were grouped in six phenotypic metaclusters based on inspection of the cluster markers genes. For the breast cancer dataset, gene expression matrices and metadata were downloaded from <http://biokey.lambrechtslab.org>. Data were normalized and filtered as done in the original

publication,⁴⁸ and the dataset was subsetted to only include CD8 T cells from baseline (untreated) samples.

We selected consensus markers of exhaustion from a comprehensive review of CD8 states from single-cell studies of human TILs.⁴⁹ The selected genes consisted of *HAVCR2*, *IFNG*, *ITGAE*, *PDCD1*, *CXCL13*, *LAYN*, *LAG3*, *TIGIT*, *CTLA4*, *ENTPD1*. This gene set was used to score individual cells with the Seurat function `AddModuleScore` with default parameters. To assess which genes display the highest positive and negative correlation with *TNFRSF9* expression, we used the R function `cor.test` with the following parameters: `method = "spearman"` and `exact = FALSE`. Genes with zero average expression were removed from the analysis. For each gene, we extracted the correlation coefficient (estimate) and the p value corrected for multiple testing.

Graphics—Figures were made in Adobe Illustrator 2022 with images generated with either GraphPad Prism 9 Software or with the following R packages: `ggplot2 v3.3.6`, `ggforce v 0.4.1`, `ggsignif v0.6.3`, `viridis v0.6.2`, `ggsci v2.9`. Graphical abstract was made with Biorender.

Supplementary Material

Refer to Web version on PubMed Central for supplementary material.

ACKNOWLEDGMENTS

We are grateful to the genotoul bioinformatics platform Toulouse Midi-Pyrenees. This work was granted access to the HPC resources of CALMIP supercomputing center under the allocation P19043. We thank Frédéric Pont, Laure Buisson, Manon Farcé, and the members from the CRCT, Infinity, and CRCL core facilities. This study has been supported by “la Fondation ARC” (PGA1–20160203788, 20180206911, 20190208630, and SIGN’IT2021); the “Institut National du Cancer” (INCA; PLBIO R16100BB, 2017–155, R19–045, R20–229); the “French National Research Agency” (ANR LABEX Toucan, AAPG 2021 R22057BB TRINDI and the EUR CARE N°ANR-18-EURE-0003); by Cancer Research Institute/Bristol-Myers Squibb CLIP grant; the Fondation Toulouse Cancer Santé; the IUCT-O translational research program; and the Intergroupe Francophone du Myélome (IFM). A.C.P. was supported by “la Ligue contre le cancer.” This work was supported in part by funding from the intramural program of NIAID, NIH.

APPENDIX

INCLUSION AND DIVERSITY

We support inclusive, diverse, and equitable conduct of research.

REFERENCES

1. Wherry EJ, and Kurachi M. (2015). Molecular and cellular insights into T cell exhaustion. *Nat. Rev. Immunol* 15, 486–499. 10.1038/nri3862. [PubMed: 26205583]
2. Pauken KE, Sammons MA, Odorizzi PM, Manne S, Godec J, Khan O, Drake AM, Chen Z, Sen DR, Kurachi M, et al. (2016). Epigenetic stability of exhausted T cells limits durability of reinvigoration by PD-1 blockade. *Science* 354, 1160–1165. 10.1126/science.aaf2807. [PubMed: 27789795]
3. Philip M, Fairchild L, Sun L, Horste EL, Camara S, Shakiba M, Scott AC, Viale A, Lauer P, Merghoub T, et al. (2017). Chromatin states define tumour-specific T cell dysfunction and reprogramming. *Nature* 545, 452–456. 10.1038/nature22367. [PubMed: 28514453]

4. Sen DR, Kaminski J, Barnitz RA, Kurachi M, Gerdemann U, Yates KB, Tsao HW, Godec J, LaFleur MW, Brown FD, et al. (2016). The epigenetic landscape of T cell exhaustion. *Science* 354, 1165–1169. 10.1126/science.aae0491. [PubMed: 27789799]
5. Thommen DS, and Schumacher TN (2018). T cell dysfunction in cancer. *Cancer Cell* 33, 547–562. 10.1016/j.ccell.2018.03.012. [PubMed: 29634943]
6. Im SJ, Hashimoto M, Gerner MY, Lee J, Kissick HT, Burger MC, Shan Q, Hale JS, Lee J, Nasti TH, et al. (2016). Defining CD8+ T cells that provide the proliferative burst after PD-1 therapy. *Nature* 537, 417–421. 10.1038/nature19330. [PubMed: 27501248]
7. Paley MA, Kroy DC, Odorizzi PM, Johnnidis JB, Dolfi DV, Barnett BE, Bikoff EK, Robertson EJ, Lauer GM, Reiner SL, and Wherry EJ (2012). Progenitor and terminal subsets of CD8+ T cells cooperate to contain chronic viral infection. *Science* 338, 1220–1225. 10.1126/science.1229620. [PubMed: 23197535]
8. Utzschneider DT, Charmoy M, Chennupati V, Pousse L, Ferreira DP, Calderon-Copete S, Danilo M, Alfei F, Hofmann M, Wieland D, et al. (2016). T cell factor 1-expressing memory-like CD8(+) T cells sustain the immune response to chronic viral infections. *Immunity* 45, 415–427. 10.1016/j.immuni.2016.07.021. [PubMed: 27533016]
9. Wu T, Ji Y, Moseman EA, Xu HC, Manglani M, Kirby M, Anderson SM, Handon R, Kenyon E, Elkahloun A, et al. (2016). The TCF1-Bcl6 axis counteracts type I interferon to repress exhaustion and maintain T cell stemness. *Sci. Immunol* 1, eaai8593. 10.1126/sciimmunol.aai8593.
10. Chen Z, Ji Z, Ngiow SF, Manne S, Cai Z, Huang AC, Johnson J, Staupe RP, Bengsch B, Xu C, et al. (2019). TCF-1-Centered Transcriptional Network Drives an Effector versus Exhausted CD8 T cell-Fate Decision. *Immunity* 51, 840–855.e5. 10.1016/j.immuni.2019.09.013. [PubMed: 31606264]
11. Khan O, Giles JR, McDonald S, Manne S, Ngiow SF, Patel KP, Werner MT, Huang AC, Alexander KA, Wu JE, et al. (2019). TOX transcriptionally and epigenetically programs CD8(+) T cell exhaustion. *Nature* 571, 211–218. 10.1038/s41586-019-1325-x. [PubMed: 31207603]
12. Scott AC, Dundar EF, Zumbo P, Chandran SS, Klebanoff CA, Shakiba M, Trivedi P, Menocal L, Appleby H, Camara S, et al. (2019). TOX is a critical regulator of tumour-specific T cell differentiation. *Nature* 571, 270–274. 10.1038/s41586-019-1324-y. [PubMed: 31207604]
13. Alfei F, Kanev K, Hofmann M, Wu M, Ghoneim HE, Roelli P, Utzschneider DT, von Hoesslin M, Cullen JG, Fan Y, et al. (2019). TOX reinforces the phenotype and longevity of exhausted T cells in chronic viral infection. *Nature* 571, 265–269. 10.1038/s41586-019-1326-9. [PubMed: 31207605]
14. Yates KB, Tonnerre P, Martin GE, Gerdemann U, Al Aboosy R, Comstock DE, Weiss SA, Wolski D, Tully DC, Chung RT, et al. (2021). Epigenetic scars of CD8(+) T cell exhaustion persist after cure of chronic infection in humans. *Nat. Immunol* 22, 1020–1029. 10.1038/s41590-021-00979-1. [PubMed: 34312547]
15. Yao C, Sun HW, Lacey NE, Ji Y, Moseman EA, Shih HY, Heuston EF, Kirby M, Anderson S, Cheng J, et al. (2019). Single-cell RNA-seq reveals TOX as a key regulator of CD8(+) T cell persistence in chronic infection. *Nat. Immunol* 20, 890–901. 10.1038/s41590-019-0403-4. [PubMed: 31209400]
16. Blank CU, Haining WN, Held W, Hogan PG, Kallies A, Lugli E, Lynn RC, Philip M, Rao A, Restifo NP, et al. (2019). Defining ‘T cell exhaustion’. *Nat. Rev. Immunol* 19, 665–674. 10.1038/s41577-019-0221-9. [PubMed: 31570879]
17. Brooks DG, Ha SJ, Elsaesser H, Sharpe AH, Freeman GJ, and Oldstone MB (2008). IL-10 and PD-L1 operate through distinct path-ways to suppress T-cell activity during persistent viral infection. *Proc. Natl. Acad. Sci. USA* 105, 20428–20433. 10.1073/pnas.0811139106. [PubMed: 19075244]
18. Tinoco R, Alcalde V, Yang Y, Sauer K, and Zuniga EI (2009). Cell-intrinsic transforming growth factor-beta signaling mediates virus-specific CD8+ T cell deletion and viral persistence in vivo. *Immunity* 31, 145–157. 10.1016/j.immuni.2009.06.015. [PubMed: 19604493]
19. Chihara N, Madi A, Kondo T, Zhang H, Acharya N, Singer M, Nyman J, Marjanovic ND, Kowalczyk MS, Wang C, et al. (2018). Induction and transcriptional regulation of the co-inhibitory gene module in T cells. *Nature* 558, 454–459. 10.1038/s41586-018-0206-z. [PubMed: 29899446]

20. Robert C, Thomas L, Bondarenko I, O'Day S, Weber J, Garbe C, Lebbe C, Baurain JF, Testori A, Grob JJ, et al. (2011). Ipilimumab plus dacarbazine for previously untreated metastatic melanoma. *N. Engl. J. Med* 364, 2517–2526. 10.1056/NEJMoa1104621. [PubMed: 21639810]
21. Topalian SL, Hodi FS, Brahmer JR, Gettinger SN, Smith DC, McDermott DF, Powderly JD, Carvajal RD, Sosman JA, Atkins MB, et al. (2012). Safety, activity, and immune correlates of anti-PD-1 antibody in cancer. *N. Engl. J. Med* 366, 2443–2454. 10.1056/NEJMoa1200690. [PubMed: 22658127]
22. Thommen DS, Koelzer VH, Herzig P, Roller A, Trefny M, Dimeloe S, Kiialainen A, Hanhart J, Schill C, Hess C, et al. (2018). A transcriptionally and functionally distinct PD-1(+) CD8(+) T cell pool with predictive potential in non-small-cell lung cancer treated with PD-1 blockade. *Nat. Med* 24, 994–1004. 10.1038/s41591-018-0057-z. [PubMed: 29892065]
23. Kurtulus S, Madi A, Escobar G, Klapholz M, Nyman J, Christian E, Pawlak M, Dionne D, Xia J, Rozenblatt-Rosen O, et al. (2019). Checkpoint blockade immunotherapy induces dynamic changes in PD-1(-)CD8(+) tumor-infiltrating T cells. *Immunity* 50, 181–194.e6. 10.1016/j.immuni.2018.11.014. [PubMed: 30635236]
24. Weulersse M, Asrir A, Pichler AC, Lemaitre L, Braun M, Carrié N, Joubert MV, Le Moine M, Do Souto L, Gaud G, et al. (2020). Eomes-dependent loss of the co-activating receptor CD226 restrains CD8(+) T cell anti-tumor functions and limits the efficacy of cancer immunotherapy. *Immunity* 53, 824–839.e10. 10.1016/j.immuni.2020.09.006. [PubMed: 33053331]
25. Braun M, Aguilera AR, Sundarajan A, Corvino D, Stannard K, Krumeich S, Das I, Lima LG, Meza Guzman LG, Li K, et al. (2020). CD155 on tumor cells drives resistance to immunotherapy by inducing the degradation of the activating receptor CD226 in CD8(+) T cells. *Immunity* 53, 805–823.e15. 10.1016/j.immuni.2020.09.010. [PubMed: 33053330]
26. Banta KL, Xu X, Chitre AS, Au-Yeung A, Takahashi C, O'Gorman WE, Wu TD, Mittman S, Cubas R, Comps-Agrar L, et al. (2022). Mechanistic convergence of the TIGIT and PD-1 inhibitory pathways necessitates co-blockade to optimize anti-tumor CD8(+) T cell responses. *Immunity* 55, 512–526.e9. 10.1016/j.immuni.2022.02.005. [PubMed: 35263569]
27. Melero I, Hirschhorn-Cymerman D, Morales-Kastresana A, Sanmamed MF, and Wolchok JD (2013). Agonist antibodies to TNFR molecules that costimulate T and NK cells. *Clin. Cancer Res* 19, 1044–1053. 10.1158/1078-0432.CCR-12-2065. [PubMed: 23460535]
28. Hurtado JC, Kim YJ, and Kwon BS (1997). Signals through 4–1BB are costimulatory to previously activated splenic T cells and inhibit activation-induced cell death. *J. Immunol* 158, 2600–2609. [PubMed: 9058792]
29. Wilcox RA, Flies DB, Zhu G, Johnson AJ, Tamada K, Chapoval AI, Strome SE, Pease LR, and Chen L. (2002). Provision of antigen and CD137 signaling breaks immunological ignorance, promoting regression of poorly immunogenic tumors. *J. Clin. Invest* 109, 651–659. 10.1172/JCI14184. [PubMed: 11877473]
30. Shuford WW, Klussman K, Tritchler DD, Loo DT, Chalupny J, Siadak AW, Brown TJ, Emswiler J, Raecho H, Larsen CP, et al. (1997). 4–1BB costimulatory signals preferentially induce CD8+ T cell proliferation and lead to the amplification in vivo of cytotoxic T cell responses. *J. Exp. Med* 186, 47–55. 10.1084/jem.186.1.47. [PubMed: 9206996]
31. Melero I, Shuford WW, Newby SA, Aruffo A, Ledbetter JA, Hellström KE, Mittler RS, and Chen L. (1997). Monoclonal antibodies against the 4–1BB T-cell activation molecule eradicate established tumors. *Nat. Med* 3, 682–685. 10.1038/nm0697-682. [PubMed: 9176498]
32. Zhu Y, Zhu G, Luo L, Flies AS, and Chen L. (2007). CD137 stimulation delivers an antigen-independent growth signal for T lymphocytes with memory phenotype. *Blood* 109, 4882–4889. 10.1182/blood-2006-10-043463. [PubMed: 17244673]
33. Guillerey C, Ferrari de Andrade L, Vuckovic S, Miles K, Ngiow SF, Yong MCR, Teng MWL, Colonna M, Ritchie DS, Chesi M, et al. (2015). Immunosurveillance and therapy of multiple myeloma are CD226 dependent. *J. Clin. Invest* 125, 2077–2089. 10.1172/JCI77181. [PubMed: 25893601]
34. Segal NH, Logan TF, Hodi FS, McDermott D, Melero I, Hamid O, Schmidt H, Robert C, Chiarion-Sileni V, Ascierto PA, et al. (2017). Results from an integrated safety analysis of urelumab, an agonist anti-CD137 monoclonal antibody. *Clin. Cancer Res* 23, 1929–1936. 10.1158/1078-0432.CCR-16-1272. [PubMed: 27756788]

35. Chester C, Sanmamed MF, Wang J, and Melero I. (2018). Immunotherapy targeting 4-1BB: mechanistic rationale, clinical results, and future strategies. *Blood* 131, 49–57. 10.1182/blood-2017-06-741041. [PubMed: 29118009]
36. Seo SK, Choi JH, Kim YH, Kang WJ, Park HY, Suh JH, Choi BK, Vinay DS, and Kwon BS (2004). 4-1BB-mediated immunotherapy of rheumatoid arthritis. *Nat. Med* 10, 1088–1094. 10.1038/nm1107. [PubMed: 15448685]
37. Choi BK, Asai T, Vinay DS, Kim YH, and Kwon BS (2006). 4-1BB-mediated amelioration of experimental autoimmune uveoretinitis is caused by indoleamine 2,3-dioxygenase-dependent mechanisms. *Cytokine* 34, 233–242. 10.1016/j.cyto.2006.04.008. [PubMed: 16899371]
38. Sun Y, Lin X, Chen HM, Wu Q, Subudhi SK, Chen L, and Fu YX (2002). Administration of agonistic anti-4-1BB monoclonal antibody leads to the amelioration of experimental autoimmune encephalomyelitis. *J. Immunol* 168, 1457–1465. 10.4049/jimmunol.168.3.1457. [PubMed: 11801689]
39. Foell J, Strahotin S, O'Neil SP, McCausland MM, Suwyn C, Haber M, Chander PN, Bapat AS, Yan XJ, Chiorazzi N, et al. (2003). CD137 costimulatory T cell receptor engagement reverses acute disease in lupus-prone NZB x NZW F1 mice. *J. Clin. Invest* 111, 1505–1518. 10.1172/JCI17662. [PubMed: 12750400]
40. Bengsch B, Ohtani T, Khan O, Setty M, Manne S, O'Brien S, Gherardini PF, Herati RS, Huang AC, Chang KM, et al. (2018). Epigenomic-guided mass cytometry profiling reveals disease-specific features of exhausted CD8 T cells. *Immunity* 48, 1029–1045.e5. 10.1016/j.immuni.2018.04.026. [PubMed: 29768164]
41. Miller BC, Sen DR, Al Abosy R, Bi K, Virkud YV, LaFleur MW, Yates KB, Lako A, Felt K, Naik GS, et al. (2019). Subsets of exhausted CD8(+) T cells differentially mediate tumor control and respond to checkpoint blockade. *Nat. Immunol* 20, 326–336. 10.1038/s41590-019-0312-6. [PubMed: 30778252]
42. Aoki T, Chong LC, Takata K, Milne K, Hav M, Colombo A, Chavez EA, Nissen M, Wang X, Miyata-Takata T, et al. (2020). Single-cell transcriptome analysis reveals disease-defining T-cell subsets in the tumor microenvironment of classic Hodgkin lymphoma. *Cancer Discov.* 10, 406–421. 10.1158/2159-8290.CD-19-0680. [PubMed: 31857391]
43. Azizi E, Carr AJ, Plitas G, Cornish AE, Konopacki C, Prabhakaran S, Nainys J, Wu K, Kiseliovas V, Setty M, et al. (2018). Single-cell map of diverse immune phenotypes in the breast tumor microenvironment. *Cell* 174, 1293–1308.e36. 10.1016/j.cell.2018.05.060. [PubMed: 29961579]
44. Guo X, Zhang Y, Zheng L, Zheng C, Song J, Zhang Q, Kang B, Liu Z, Jin L, Xing R, et al. (2018). Global characterization of T cells in non-small-cell lung cancer by single-cell sequencing. *Nat. Med* 24, 978–985. 10.1038/s41591-018-0045-3. [PubMed: 29942094]
45. Sade-Feldman M, Yizhak K, Bjorgaard SL, Ray JP, de Boer CG, Jenkins RW, Lieb DJ, Chen JH, Frederick DT, Barzily-Rokni M, et al. (2018). Defining T cell states associated with response to check-point immunotherapy in melanoma. *Cell* 175, 998–1013.e20. 10.1016/j.cell.2018.10.038. [PubMed: 30388456]
46. Zheng C, Zheng L, Yoo JK, Guo H, Zhang Y, Guo X, Kang B, Hu R, Huang JY, Zhang Q, et al. (2017). Landscape of infiltrating T cells in liver cancer revealed by single-cell sequencing. *Cell* 169, 1342–1356.e16. 10.1016/j.cell.2017.05.035. [PubMed: 28622514]
47. Lucca LE, Axisa PP, Lu B, Harnett B, Jessel S, Zhang L, Raddassi K, Zhang L, Olino K, Clune J, et al. (2021). Circulating clonally expanded T cells reflect functions of tumor-infiltrating T cells. *J. Exp. Med* 218, e20200921. 10.1084/jem.20200921.
48. Bassez A, Vos H, Van Dyck L, Floris G, Arijis I, Desmedt C, Boeckx B, Vanden Bempt M, Nevelsteen I, Lambein K, et al. (2021). A single-cell map of intratumoral changes during anti-PD1 treatment of patients with breast cancer. *Nat. Med* 27, 820–832. 10.1038/s41591-021-01323-8. [PubMed: 33958794]
49. van der Leun AM, Thommen DS, and Schumacher TN (2020). CD8(+) T cell states in human cancer: insights from single-cell analysis. *Nat. Rev. Cancer* 20, 218–232. 10.1038/s41568-019-0235-4. [PubMed: 32024970]
50. Siddiqui I, Schaeuble K, Chennupati V, Fuertes Marraco SA, Calderon-Copete S, Pais Ferreira D, Carmona SJ, Scarpellino L, Gfeller D, Pradervand S, et al. (2019). Intratumoral Tcf1(+)PD-1(+) CD8(+) T cells with stem-like properties promote tumor control in response to

vaccination and checkpoint blockade immunotherapy. *Immunity* 50, 195–211.e10 e110. 10.1016/j.immuni.2018.12.021.

51. Utzschneider DT, Gabriel SS, Chisanga D, Gloury R, Gubser PM, Vasanthakumar A, Shi W, and Kallies A. (2020). Early precursor T cells establish and propagate T cell exhaustion in chronic infection. *Nat. Immunol* 21, 1256–1266. 10.1038/s41590-020-0760-z. [PubMed: 32839610]
52. Giles JR, Ngiow SF, Manne S, Baxter AE, Khan O, Wang P, Staupe R, Abdel-Hakeem MS, Huang H, Mathew D, et al. (2022). Shared and distinct biological circuits in effector, memory and exhausted CD8(+) T cells revealed by temporal single-cell transcriptomics and epigenetics. *Nat. Immunol* 23, 1600–1613. 10.1038/s41590-022-01338-4. [PubMed: 36271148]
53. Guillerey C, Harjunpää H, Carrié N, Kassem S, Teo T, Miles K, Krumeich S, Weulersse M, Cuisinier M, Stannard K, et al. (2018). TIGIT immune checkpoint blockade restores CD8(+) T-cell immunity against multiple myeloma. *Blood* 132, 1689–1694. 10.1182/blood-2018-01-825265. [PubMed: 29986909]
54. Qi X, Li F, Wu Y, Cheng C, Han P, Wang J, and Yang X. (2019). Optimization of 4–1BB antibody for cancer immunotherapy by balancing agonistic strength with FcγR3 affinity. *Nat. Commun* 10, 2141. 10.1038/s41467-019-10088-1. [PubMed: 31105267]
55. Lee HW, Park SJ, Choi BK, Kim HH, Nam KO, and Kwon BS (2002). 4–1BB promotes the survival of CD8+ T lymphocytes by increasing expression of Bcl-xL and Bfl-1. *J. Immunol* 169, 4882–4888. [PubMed: 12391199]
56. Sabbagh L, Andreeva D, Laramée GD, Oussa NA, Lew D, Bisson N, Soumounou Y, Pawson T, and Watts TH (2013). Leukocyte-specific protein 1 links TNF receptor-associated factor 1 to survival signaling downstream of 4–1BB in T cells. *J. Leukoc. Biol* 93, 713–721. 10.1189/jlb.1112579. [PubMed: 23446150]
57. Lages CS, Lewkowich I, Sproles A, Wills-Karp M, and Chougnet C. (2010). Partial restoration of T-cell function in aged mice by in vitro blockade of the PD-1/PD-L1 pathway. *Aging Cell* 9, 785–798. 10.1111/j.1474-9726.2010.00611.x. [PubMed: 20653631]
58. Lee KA, Shin KS, Kim GY, Song YC, Bae EA, Kim IK, Koh CH, and Kang CY (2016). Characterization of age-associated exhausted CD8(+) T cells defined by increased expression of Tim-3 and PD-1. *Aging Cell* 15, 291–300. 10.1111/ace.12435. [PubMed: 26750587]
59. Garcia MG, Deng Y, Murray C, Reyes RM, Padron A, Bai H, Kancharla A, Gupta H, Shen-Orr S, and Curiel TJ (2022). Immune checkpoint expression and relationships to anti-PD-L1 immune check-point blockade cancer immunotherapy efficacy in aged versus young mice. *Aging Cancer* 3, 68–83. 10.1002/aac2.12045. [PubMed: 36876140]
60. Martinez GJ, Pereira RM, Aijö T, Kim EY, Marangoni F, Pipkin ME, Togher S, Heissmeyer V, Zhang YC, Crotty S, et al. (2015). The transcription factor NFAT promotes exhaustion of activated CD8(+) T cells. *Immunity* 42, 265–278. 10.1016/j.immuni.2015.01.006. [PubMed: 25680272]
61. Moran AE, Holzapfel KL, Xing Y, Cunningham NR, Maltzman JS, Punt J, and Hogquist KA (2011). T cell receptor signal strength in Treg and iNKT cell development demonstrated by a novel fluorescent reporter mouse. *J. Exp. Med* 208, 1279–1289. 10.1084/jem.20110308. [PubMed: 21606508]
62. Borchering N, Bormann NL, and Kraus G. (2020). scRepertoire: an R-based toolkit for single-cell immune receptor analysis. *F1000Res* 9, 47. 10.12688/f1000research.22139.2. [PubMed: 32789006]
63. Zhang L, Yu X, Zheng L, Zhang Y, Li Y, Fang Q, Gao R, Kang B, Zhang Q, Huang JY, et al. (2018). Lineage tracking reveals dynamic relationships of T cells in colorectal cancer. *Nature* 564, 268–272. 10.1038/s41586-018-0694-x. [PubMed: 30479382]
64. Maurice NJ, Berner J, Taber AK, Zehn D, and Pricl M. (2021). Inflammatory signals are sufficient to elicit TOX expression in mouse and human CD8+ T cells. *JCI Insight* 6, e150744. 10.1172/jci.insight.150744.
65. Zapata JM, Perez-Chacon G, Carr-Baena P, Martinez-Forero I, Azpilikueta A, Otano I, and Melero I. (2018). CD137 (4–1BB) signalosome: complexity is a matter of TRAFs. *Front. Immunol* 9, 2618. 10.3389/fimmu.2018.02618. [PubMed: 30524423]

66. Grinberg-Bleyer Y, Oh H, Desrichard A, Bhatt DM, Caron R, Chan TA, Schmid RM, Klein U, Hayden MS, and Ghosh S. (2017). NF-kappaB c-Rel is crucial for the regulatory T cell immune checkpoint in cancer. *Cell* 170, 1096–1108.e13. 10.1016/j.cell.2017.08.004. [PubMed: 28886380]
67. Oh H, Grinberg-Bleyer Y, Liao W, Maloney D, Wang P, Wu Z, Wang J, Bhatt DM, Heise N, Schmid RM, et al. (2017). An NF-kappaB transcription-factor-dependent lineage-specific transcriptional program promotes regulatory T cell identity and function. *Immunity* 47, 450–465.e5. 10.1016/j.immuni.2017.08.010. [PubMed: 28889947]
68. Lalle G, Lautreite R, Voisin A, Twardowski J, Stéphan P, Perrin-Niquet M, Igalouzene R, Soudja SM, Marie JC, Vocanson M, et al. (2021). A T cell-intrinsic function for NF-kappaB RelB in experimental autoimmune encephalomyelitis. *Sci. Rep* 11, 19674. 10.1038/s41598-021-99134-x. [PubMed: 34608221]
69. Mognol GP, Spreafico R, Wong V, Scott-Browne JP, Togher S, Hoffmann A, Hogan PG, Rao A, and Trifari S. (2017). Exhaustion-associated regulatory regions in CD8(+) tumor-infiltrating T cells. *Proc. Natl. Acad. Sci. USA* 114, E2776–E2785. 10.1073/pnas.1620498114. [PubMed: 28283662]
70. Scott-Browne JP, López-Moyado IF, Trifari S, Wong V, Chavez L, Rao A, and Pereira RM (2016). Dynamic changes in chromatin accessibility occur in CD8(+) T cells responding to viral. *Immunity* 45, 1327–1340. 10.1016/j.immuni.2016.10.028. [PubMed: 27939672]
71. Schep AN, Wu B, Buenrostro JD, and Greenleaf WJ (2017). chromVAR: inferring transcription-factor-associated accessibility from single-cell epigenomic data. *Nat. Methods* 14, 975–978. 10.1038/nmeth.4401. [PubMed: 28825706]
72. Asrir A, Tardiveau C, Coudert J, Laffont R, Blanchard L, Bellard E, Veerman K, Bettini S, Lafouresse F, Vina E, et al. (2022). Tumor-associated high endothelial venules mediate lymphocyte entry into tumors and predict response to PD-1 plus CTLA-4 combination immunotherapy. *Cancer Cell* 40, 318–334.e9. 10.1016/j.ccell.2022.01.002. [PubMed: 35120598]
73. Guillerey C, Nakamura K, Pichler AC, Barkauskas D, Krumeich S, Stannard K, Miles K, Harjunpää H, Yu Y, Casey M, et al. (2019). Chemotherapy followed by anti-CD137 mAb immunotherapy improves disease control in a mouse myeloma model. *JCI Insight* 5, e125932. 10.1172/jci.insight.125932. [PubMed: 31194697]
74. Bucks CM, Norton JA, Boesteanu AC, Mueller YM, and Katsikis PD (2009). Chronic antigen stimulation alone is sufficient to drive CD8+ T cell exhaustion. *J. Immunol* 182, 6697–6708. 10.4049/jimmunol.0800997. [PubMed: 19454664]
75. Ward-Kavanagh LK, Lin WW, Šedý JR, and Ware CF (2016). The TNF receptor superfamily in co-stimulating and co-inhibitory responses. *Immunity* 44, 1005–1019. 10.1016/j.immuni.2016.04.019. [PubMed: 27192566]
76. Pulle G, Vidric M, and Watts TH (2006). IL-15-dependent induction of 4–1BB promotes antigen-independent CD8 memory T cell survival. *J. Immunol* 176, 2739–2748. 10.4049/jimmunol.176.5.2739. [PubMed: 16493029]
77. Lin GH, Snell LM, Wortzman ME, Clouthier DL, and Watts TH (2013). GITR-dependent regulation of 4–1BB expression: implications for T cell memory and anti-4–1BB-induced pathology. *J. Immunol* 190, 4627–4639. 10.4049/jimmunol.1201854. [PubMed: 23536631]
78. Palazón A, Martínez-Forero I, Teijeira A, Morales-Kastresana A, Alfaro C, Sanmamed MF, Perez-Gracia JL, Peñuelas I, Hervás-Stubbs S, Rouzaut A, et al. (2012). The HIF-1alpha hypoxia response in tumor-infiltrating T lymphocytes induces functional CD137 (4–1BB) for immunotherapy. *Cancer Discov.* 2, 608–623. 10.1158/2159-8290.CD-11-0314. [PubMed: 22719018]
79. Cai C, Samir J, Pirozyan MR, Adikari TN, Gupta M, Leung P, Hughes B, Van der Byl W, Rizzetto S, Elthala A, et al. (2022). Identification of human progenitors of exhausted CD8(+) T cells associated with elevated IFN-gamma response in early phase of viral infection. *Nat. Commun* 13, 7543. 10.1038/s41467-022-35281-7. [PubMed: 36477661]
80. Galletti G, De Simone G, Mazza EMC, Puccio S, Mezzanotte C, Bi TM, Davydov AN, Metsger M, Scamardella E, Alvisi G, et al. (2020). Two subsets of stem-like CD8(+) memory T cell progenitors with distinct fate commitments in humans. *Nat. Immunol* 21, 1552–1562. 10.1038/s41590-020-0791-5. [PubMed: 33046887]

81. Hensel N, Gu Z, Sagar X, Wieland D, Jechow K, Kemming J, Llewellyn-Lacey S, Gostick E, Sogukpinar O, Emmerich F, et al. (2021). Memory-like HCV-specific CD8(+) T cells retain a molecular scar after cure of chronic HCV infection. *Nat. Immunol* 22, 229–239. 10.1038/s41590-020-00817-w. [PubMed: 33398179]
82. Etxeberria I, Bolaños E, Teijeira A, Garasa S, Yanguas A, Azpilikueta A, Kavanaugh WM, Vasiljeva O, Belvin M, Howng B, et al. (2021). Antitumor efficacy and reduced toxicity using an anti-CD137 Probody therapeutic. *Proc. Natl. Acad. Sci. USA* 118, e2025930118. 10.1073/pnas.2025930118.
83. Geuijen C, Tacke P, Wang LC, Klooster R, van Loo PF, Zhou J, Mondal A, Liu YB, Kramer A, Condamine T, et al. (2021). A human CD137xPD-L1 bispecific antibody promotes anti-tumor immunity via context-dependent T cell costimulation and checkpoint blockade. *Nat. Commun* 12, 4445. 10.1038/s41467-021-24767-5. [PubMed: 34290245]
84. Schmitz JE, Kuroda MJ, Santra S, Sasseville VG, Simon MA, Lifton MA, Racz P, Tenner-Racz K, Dalesandro M, Scallon BJ, et al. (1999). Control of viremia in simian immunodeficiency virus infection by CD8+ lymphocytes. *Science* 283, 857–860. 10.1126/science.283.5403.857. [PubMed: 9933172]
85. Yost KE, Satpathy AT, Wells DK, Qi Y, Wang C, Kageyama R, McNamara KL, Granja JM, Sarin KY, Brown RA, et al. (2019). Clonal replacement of tumor-specific T cells following PD-1 blockade. *Nat. Med* 25, 1251–1259. 10.1038/s41591-019-0522-3. [PubMed: 31359002]
86. Salih HR, Kosowski SG, Haluska VF, Starling GC, Loo DT, Lee F, Aruffo AA, Trail PA, and Kiener PA (2000). Constitutive expression of functional 4–1BB (CD137) ligand on carcinoma cells. *J. Immunol* 165, 2903–2910. 10.4049/jimmunol.165.5.2903. [PubMed: 10946324]
87. Porgador A, Feldman M, and Eisenbach L. (1989). H-2Kb transfection of B16 melanoma cells results in reduced tumorigenicity and metastatic competence. *J. Immunogenet* 16, 291–303. 10.1111/j.1744-313x.1989.tb00475.x. [PubMed: 2639904]
88. Trimaglio G, Tilkin-Mariamé A-F, Feliu V, Lauzéral-Vizcaino F, Tosolini M, Valle C, Ayyoub M, Neyrolles O, Vergnolle N, Rombouts Y, et al. (2020). Colon-specific immune microenvironment regulates cancer progression versus rejection. *OncoImmunology* 9. 10.1080/2162402X.2020.1790125.
89. Chesi M, Matthews GM, Garbitt VM, Palmer SE, Shortt J, Lefebure M, Stewart AK, Johnstone RW, and Bergsagel PL (2012). Drug response in a genetically engineered mouse model of multiple myeloma is predictive of clinical efficacy. *Blood* 120, 376–385. 10.1182/blood-2012-02-412783. [PubMed: 22451422]
90. Nakamura K, Kassem S, Cleynen A, Chrétien M-L, Guillerey C, Putz EM, Bald T, Förster I, Vuckovic S, Hill GR, et al. (2018). Dysregulated IL-18 Is a Key Driver of Immunosuppression and a Possible Therapeutic Target in the Multiple Myeloma Microenvironment. *Cancer Cell* 33, 634–648.e5. 10.1016/j.ccell.2018.02.007. [PubMed: 29551594]
91. Dobin A, Davis CA, Schlesinger F, Drenkow J, Zaleski C, Jha S, Batut P, Chaisson M, and Gingeras TR (2013). STAR: ultrafast universal RNA-seq aligner. *Bioinformatics* 29, 15–21. 10.1093/bioinformatics/bts635. [PubMed: 23104886]
92. Liao Y, Smyth GK, and Shi W. (2014). featureCounts: an efficient general purpose program for assigning sequence reads to genomic features. *Bioinformatics* 30, 923–930. 10.1093/bioinformatics/btt656. [PubMed: 24227677]
93. Ritchie ME, Phipson B, Wu D, Hu Y, Law CW, Shi W, and Smyth GK (2015). limma powers differential expression analyses for RNA-sequencing and microarray studies. *Nucleic Acids Research* 43, e47. 10.1093/nar/gkv007. [PubMed: 25605792]
94. Polit L, Kerdivel G, Gregoricchio S, Esposito M, Guillouf C, and Boeva V. (2021). CHIPIN: ChIP-seq inter-sample normalization based on signal invariance across transcriptionally constant genes. *BMC Bioinformatics* 22, 407. 10.1186/s12859-021-04320-3. [PubMed: 34404353]
95. Love MI, Huber W, and Anders S. (2014). Moderated estimation of fold change and dispersion for RNA-seq data with DESeq2. *Genome Biol.* 15, 550. 10.1186/s13059-014-0550-8. [PubMed: 25516281]
96. Chesi M, Robbiani DF, Sebag M, Chng WJ, Affer M, Tiedemann R, Valdez R, Palmer SE, Haas SS, Stewart AK, et al. (2008). AID-dependent activation of a MYC transgene induces multiple

- myeloma in a conditional mouse model of post-germinal center malignancies. *Cancer Cell* 13, 167–180. 10.1016/j.ccr.2008.01.007. [PubMed: 18242516]
97. Adoue V, Binet B, Malbec A, Fourquet J, Romagnoli P, van Meerwijk JPM, Amigorena S, and Joffe OP (2019). The histone methyltransferase SETDB1 controls T helper cell lineage integrity by repressing endogenous retroviruses. *Immunity* 50, 629–644.e8. 10.1016/j.immuni.2019.01.003. [PubMed: 30737147]
98. Stoeckius M, Hafemeister C, Stephenson W, Houck-Loomis B, Chattopadhyay PK, Swerdlow H, Satija R, and Smibert P. (2017). Simultaneous epitope and transcriptome measurement in single cells. *Nat. Methods* 14, 865–868. 10.1038/nmeth.4380. [PubMed: 28759029]
99. Pont F, Tosolini M, and Fournié JJ (2019). Single-Cell Signature Explorer for comprehensive visualization of single cell signatures across scRNA-seq datasets. *Nucleic Acids Res.* 47, e133. 10.1093/nar/gkz601. [PubMed: 31294801]
100. Liberzon A, Birger C, Thorvaldsdóttir H, Ghandi M, Mesirov JP, and Tamayo P. (2015). The Molecular Signatures Database (MSigDB) hallmark gene set collection. *Cell Syst.* 1, 417–425. 10.1016/j.cels.2015.12.004. [PubMed: 26771021]
101. Burkhardt DB, Stanley JS 3rd, Tong A, Perdigoto AL, Gigante SA, Herold KC, Wolf G, Giraldez AJ, van Dijk D, and Krishnaswamy S. (2021). Quantifying the effect of experimental perturbations at single-cell resolution. *Nat. Biotechnol* 39, 619–629. 10.1038/s41587-020-00803-5. [PubMed: 33558698]
102. Lopez-Delisle L, Rabbani L, Wolff J, Bhardwaj V, Backofen R, Grüning B, Ramírez F, and Manke T. (2021). pyGenomeTracks: reproducible plots for multivariate genomic datasets. *Bioinformatics* 37, 422–423. 10.1093/bioinformatics/btaa692. [PubMed: 32745185]
103. Krämer A, Green J, Pollard J Jr., and Tugendreich S. (2014). Causal analysis approaches in Ingenuity Pathway Analysis. *Bioinformatics* 30, 523–530. 10.1093/bioinformatics/btt703. [PubMed: 24336805]
104. Fornes O, Castro-Mondragon JA, Khan A, van der Lee R, Zhang X, Richmond PA, Modi BP, Correard S, Gheorghe M, Baranaši D, et al. (2020). JASPAR 2020: update of the open-access database of transcription factor binding profiles. *Nucleic Acids Res.* 48, D87–D92. 10.1093/nar/gkz1001. [PubMed: 31701148]

Highlights

- T cell-specific deletion of CD137 limits the presence of CD8⁺ Tex cells in tumors
- NF- κ B-dependent CD137 signaling stimulates Tex cell proliferation and differentiation
- CD137 activation drives the Tox-dependent epigenetic remodeling of Tex cell genes
- Anti-PD1 efficacy is improved by subsequent CD137 stimulation

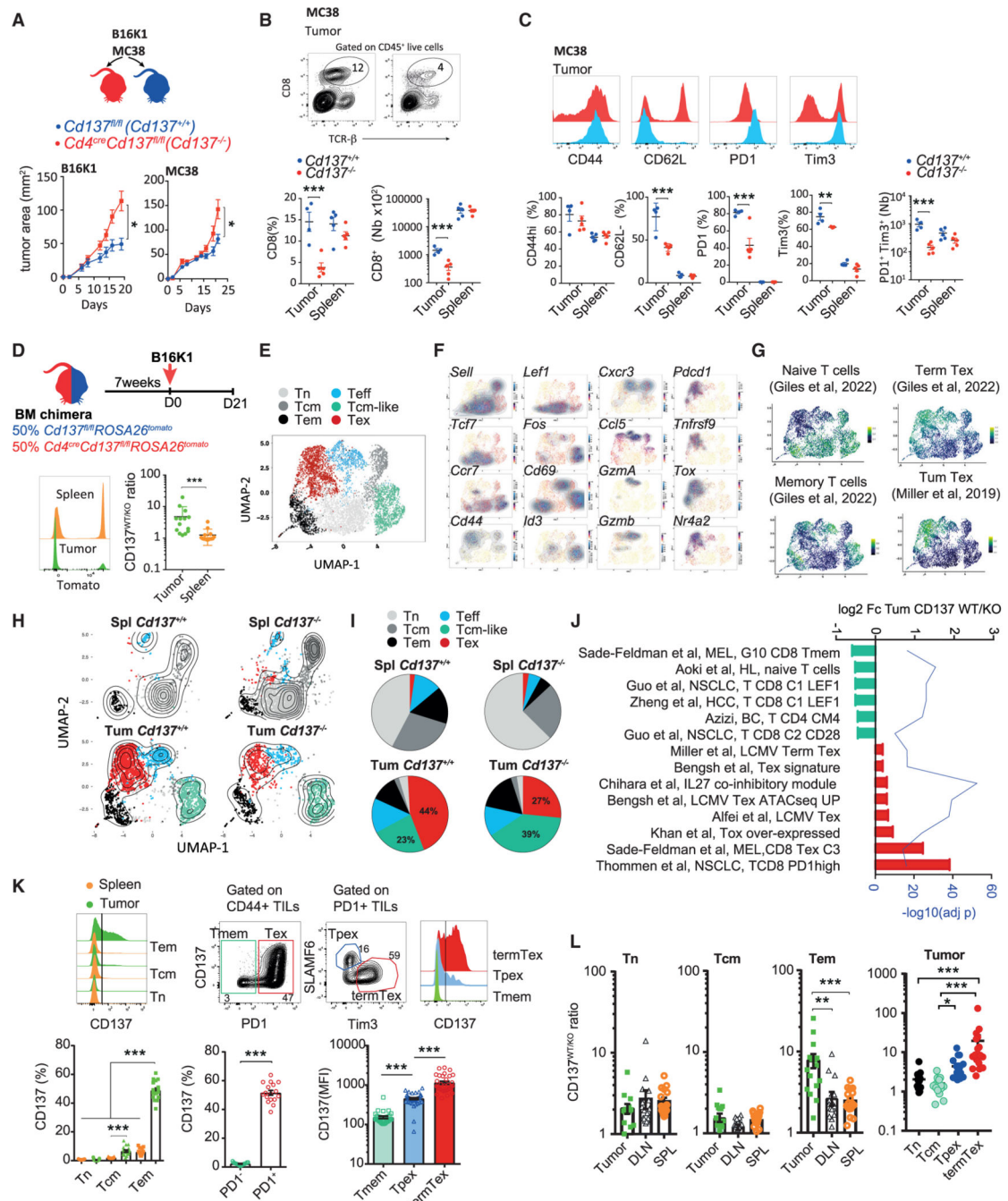


Figure 1. CD137 deficiency limits tumor-infiltrating Tex cells

(A–C) $Cd4^{cre}Cd137^{fl/fl}$ ($Cd137^{-/-}$) and $Cd137^{fl/fl}$ ($Cd137^{+/+}$) were injected s.c. with MC38 or B16K1 cells. (A) Tumor area. (B) Frequency and number of CD8⁺ T cells. (C) Expression of the indicated markers by CD8⁺ T cells. (D–J) $Cd4^{cre}Cd137^{fl/fl}ROSA26^{tomato}$ and $Cd137^{fl/fl}ROSA26^{tomato}$ mixed BM chimeras were injected s.c. with B16K1 cells. $Cd137^{-/-}$ (tomato⁺) and $Cd137^{+/+}$ (tomato⁻) spleen and tumor-infiltrating CD8⁺ T cells were analyzed by single-cell RNA sequencing (scRNA-seq) after 21 days. (n = 7 pooled mice/group.) (D) Ratio of $CD137^{+/+}$ vs. $CD137^{-/-}$

(CD137^{WT/KO}) spleen and tumor-infiltrating CD8⁺ T cells. (E) Spleen and tumor-infiltrating CD8⁺ T cells transcriptomic landscape scattered in 6 clusters. (F and G) Relative expression of the indicated genes (F) and signatures (G).

(H and I) UMAP (H) and graphs (I) showing cluster frequency in the indicated samples.

(J) Fold change in expression and adjusted p value of relevant pathways enriched in *Cd137^{+/+}* vs. *Cd137^{-/-}* tumor-infiltrating CD8⁺ T cells.

(K) Expression of CD137 by the indicated spleen or B16K1-tumor-infiltrating CD8⁺ T cell subsets after 19 days.

(L) CD137^{WT/KO} ratio in the indicated CD8⁺ T cell subsets from B16K1 bearing mixed BM chimeras as in (D). Data are presented as mean ± SEM from at least 2 independent experiments. Each symbol represents an individual mouse. *p < 0.05; **p < 0.01, ***p < 0.001 (Mann-Whitney test or ANOVA with Tukey's post-test analysis).

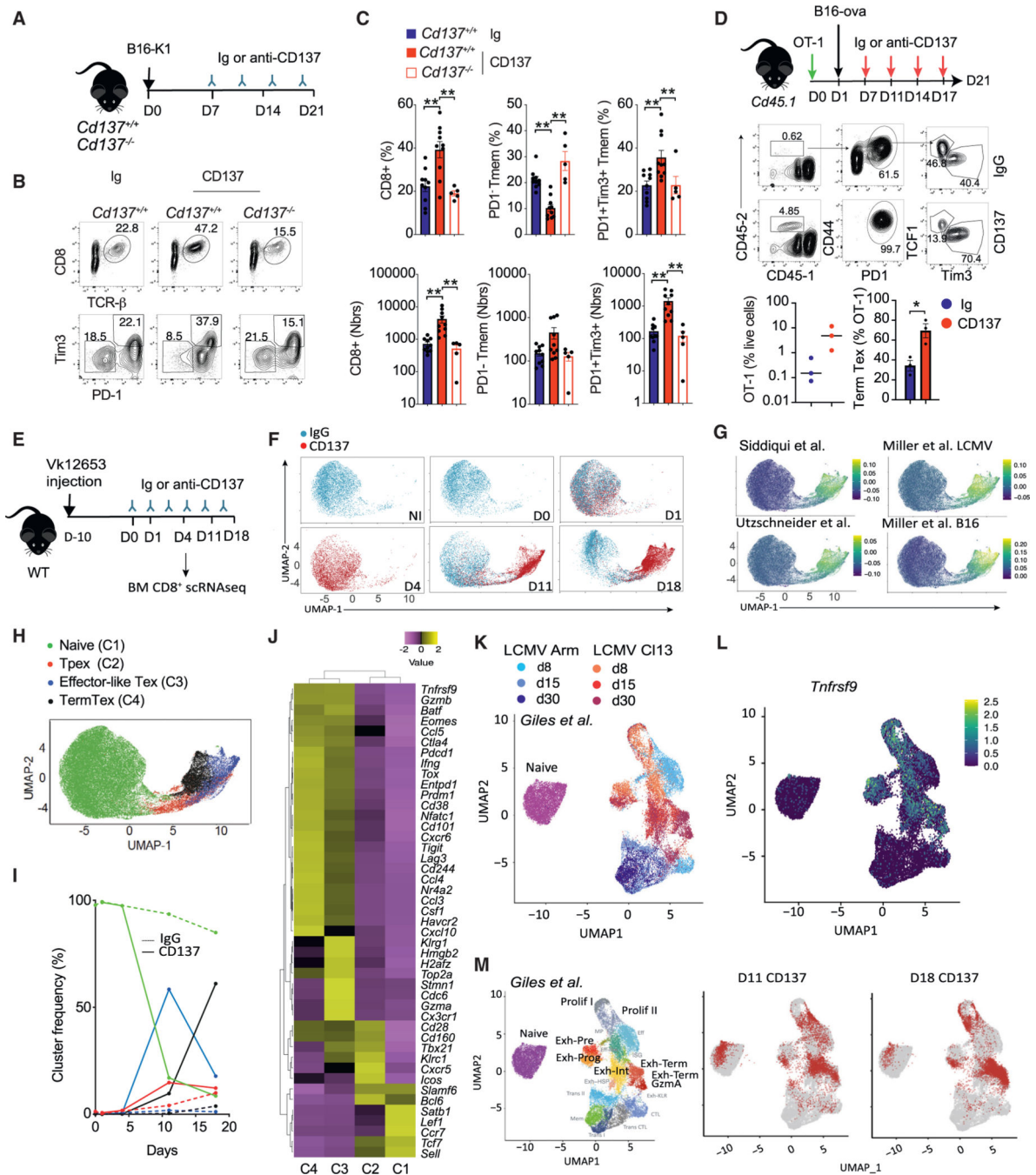


Figure 2. CD137 stimulation favors tumor Tex cell accumulation

(A–C) $Cd4^{cre}Cd137^{fl/fl}$ ($Cd137^{-/-}$) and $Cd137^{fl/fl}$ ($Cd137^{+/+}$) were injected s.c. with B16K1 cells and treated with anti-CD137 (3H3, 10 μ g) or Ig control mAbs. (A) Experimental design. (B and C) FACS plots (B) and graphs (C) showing the frequency and numbers of PD1⁺Tim3⁺ CD8⁺TILs after 21 days.

(D) $Cd45.1$ mice reconstituted with 10^7 OT-1 cells were injected B16-ova tumors and treated with anti-CD137 or Ig mAbs. Experimental design and graphs showing the intratumor Tpex and TermTex OT-1 CD8⁺ T cells frequency.

(E–J) WT mice were challenged with Vk12653 myeloma cells and after 10 days, mice were injected with anti-CD137 or Ig mAbs. Bone marrow CD8⁺ T cells were analyzed by scRNA-seq (n = 5 pooled mice/group). (E) Experimental design. (F) UMAP split by Ig or anti-CD137 treatment. (G) Relative expression of the indicated Tex-specific signature.^{41,50,51} (H) Identification of four clusters on UMAP plots. (I) Frequency of the indicated clusters along Ig or anti-CD137 treatment.

(J) Log-normalized gene-expression heatmap showing the expression of naive, T_{pex}, effector-like, and TermTex cell signature genes by the indicated clusters defined as in (H). Data are scaled rowwise (violet low – yellow high).

(K–M) Comparison of anti-CD137 scRNA-seq as in (E) with Giles et al.⁵² dataset of CD8⁺ T cells from LCMV Arm and cl13. (K) UMAP plot colored by experimental conditions.

(L) Relative expression of *Tnfrsf9*. (M) Left, UMAP plot colored by transcriptional clusters of interest. Center and right, projection of the indicated anti-CD137-treated CD8⁺ T cells over UMAP coordinates. Data are presented as mean ± SEM from at least 2 independent experiments. Each symbol represents an individual mouse. *p < 0.05; **p < 0.01, ***p < 0.001 (Student's t test or ANOVA with Tukey's post-test analysis).

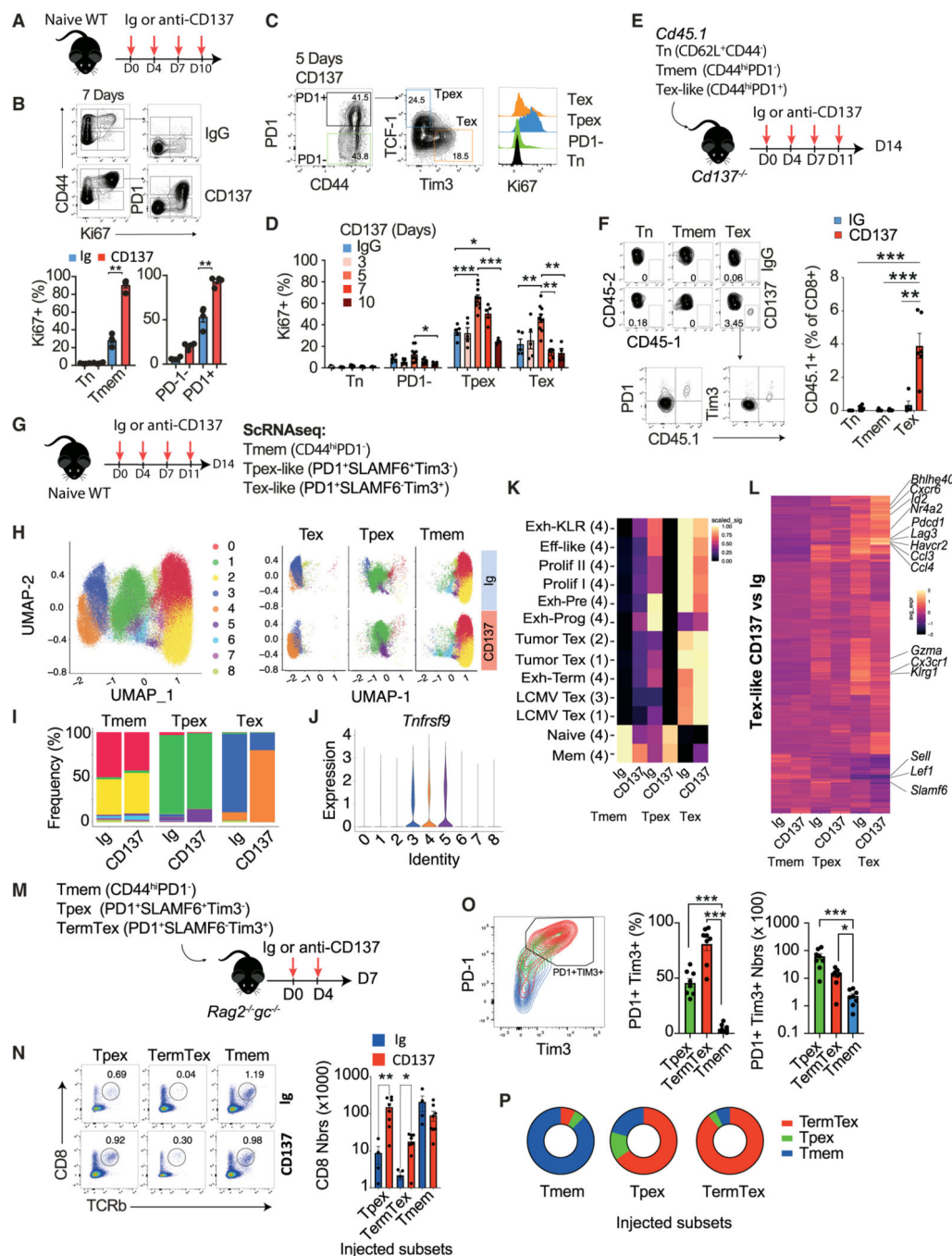


Figure 3. CD137 promotes Tex cell expansion and differentiation

(A–D) Naive WT mice were treated with anti-CD137 (3H3, 10 μg) or IgG control mAbs.

(A) Experimental design. (B–D) FACS plot and graphs showing Ki-67 expression by the indicated CD8⁺ T cell subsets along treatment.

(E and F) The indicated CD45.1 CD8⁺ T cell subsets were injected i.v. into *Cd137*^{-/-} mice that were treated with anti-CD137 or IgG. (E) Experimental design. (F) FACS plot and graphs showing the frequency of CD45.1⁺ CD8⁺ T cells after 14 days.

(G–K) WT mice were injected with anti-CD137 or IgG. The indicated splenic CD8⁺ T cell subsets were analyzed by scRNA-seq (n = 5–10 pooled mice/group). (G) Experimental design. (H and I) UMAP (H) and bar plots (I) showing CD8⁺ T cell cluster distribution. (J) Relative expression of *Tnfrsf9*. (K) Clustered heatmap showing the indicated signature expression (1: Miller et al.⁴¹; 2: Siddiqui et al.⁵⁰; 3: Utzschneider et al.⁵¹; 4: Giles et al.⁵²). Data are scaled rowwise.

(L) Clustered heatmap showing the 280 differentially expressed genes between Tex-like cells treated with anti-CD137 or Ig ($\log_2FC > 0.25$).

(M–P) The indicated CD8⁺ T cell subsets isolated from WT mice treated with anti-CD137 were injected i.v. into *Rag2*^{-/-}*Il2rg*^{-/-} mice treated with anti-CD137 or IgG. (M) Experimental design. (N) FACS plots and numbers of CD8⁺ T cells recovered after 7 days. (O) FACS plots and graphs showing PD1 and Tim3 expression and numbers. (P) Frequency of CD8⁺ T cells with a Tmem (CD44^{hi}PD1⁻), Tpex (PD1⁺TCF1⁺Tim3⁻), or TermTex (PD1⁺TCF1⁻Tim3⁺) cell phenotype. Data are presented as mean \pm SEM from at least 2 independent experiments. Each symbol represents an individual mouse. *p < 0.05; **p < 0.01, ***p < 0.001 (paired t test or ANOVA with Tukey's post-test analysis).

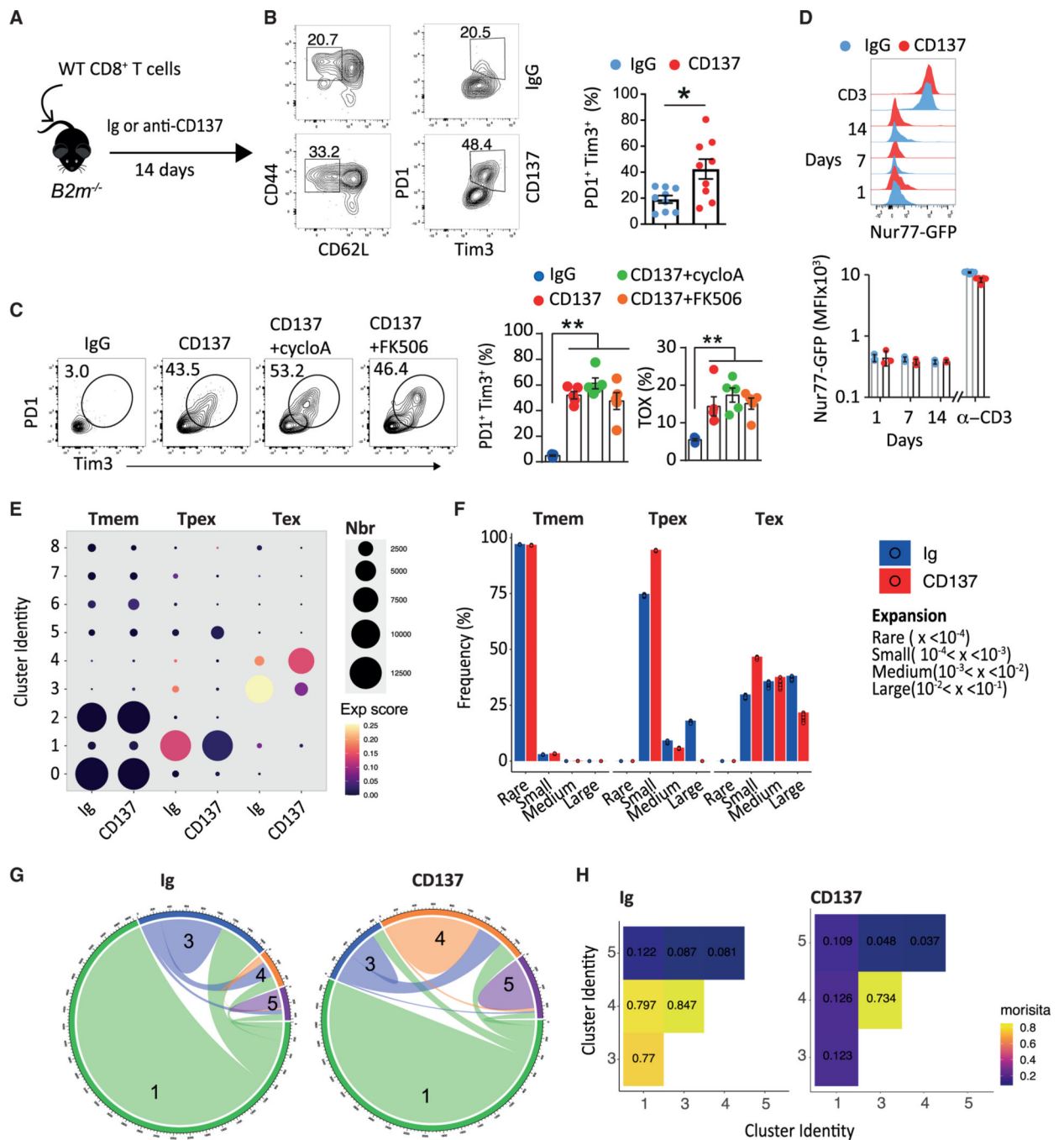


Figure 4. CD137-induced Tex cell expansion does not require TCR/calcineurin signaling pathway

(A and B) WT CD8⁺ T cells were transferred into *B2m*^{-/-} mice subsequently treated with anti-CD137 (10 μg; 3H3, i.p. twice a week) or Ig mAbs. (A) Experimental design. (B) Frequency of splenic PD1⁺Tim3⁺ CD8⁺ Tem cells.

(C) WT mice were treated with cyclosporin A or FK506 in combination with anti-CD137 or Ig. Frequency of Tim3⁺PD1⁺ or Tox⁺ CD8⁺ Tem cells.

(D) Nur77^{GFP} mice were treated with anti-CD137 or IgG for the indicated period. Expression of GFP by CD8⁺ Tem cells after 1, 7, and 14 days of treatment or upon 24 h of anti-CD3+CD28 *in vitro*.

(E) Shannon entropy-based expansion score of clusters from Figure 3H. Color of the dots indicates the intensity of the score and size the number of cells.

(F) Frequency of CD8⁺ T cells according to their expansion between subsets and treatments. Each dot represents a resampling of the original dataset equivalent to 90% of the smallest treatment-subset sample.

(G and H) Clonal overlap between the main Tpex and Tex clusters. Circos plots (G) and Morisita index (H). Data are presented as mean \pm SEM from at least 2 independent experiments. Each symbol represents an individual mouse. *p < 0.05; **p < 0.01, ***p < 0.001 (Mann-Whitney or ANOVA with Tukey's post-test analysis).

(F and G) Frequency of splenic PD1⁺Tim3⁺ CD8⁺ Tem cells in *Cd4cre*^{+/-} control mice and *Cd4cre*^{+/-} crossed with *Rela*^{fl/fl}, *Rel*^{fl/fl}, *Relb*^{fl/fl}, or *Nfkb2*^{fl/fl} mice treated with anti-CD137 or IgG for 18 days.

(H–J) scRNA-seq as in Figure 2F.

(H) Relative expression of NF-κB target gene signature.

(I) *In silico* gating of PD1⁻Tim3⁻ double-negative (DN), PD1⁺ simple-positive (SP), and PD1⁺Tim3⁺ double-positive (DP) cells and their numbers in the different Ig or anti-CD137 conditions.

(J) Relative expression of the NF-κB target gene signature.

(K) UMAP and violin plot comparing NF-κB target gene signature in CD8⁺ T cell subsets as in Figure 3H.

(L) Violin plot comparing NF-κB target gene signatures in *Cd137*^{-/-} and *Cd137*^{+/+} CD8⁺ T cell subsets as in Figure 1E. Data are presented as mean ± SEM from at least 2 independent experiments. Each symbol represents an individual mouse. *p < 0.05; **p < 0.01, ***p < 0.001 (Mann-Whitney, paired t test or ANOVA with Tukey's post-test analysis).

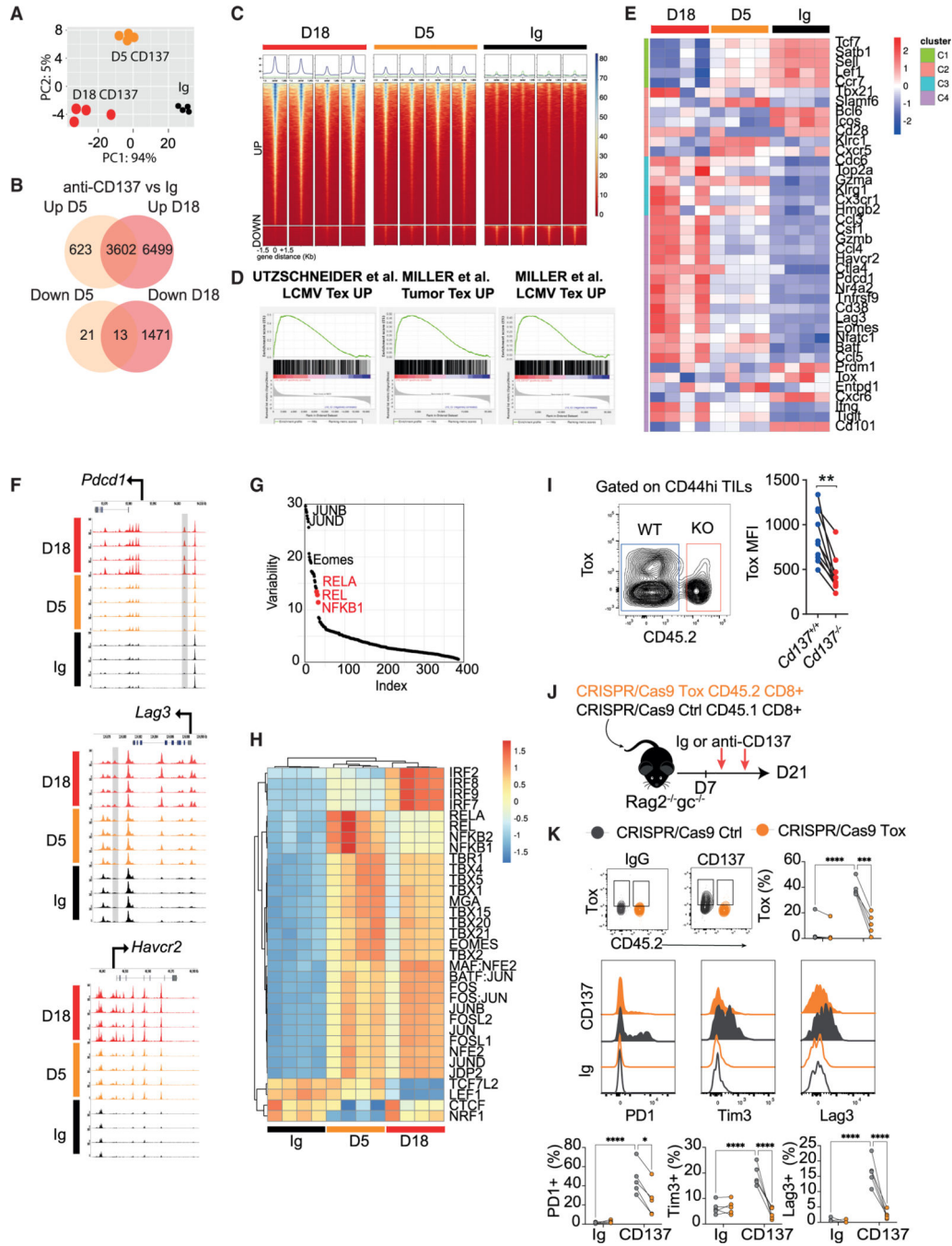


Figure 6. Anti-CD137 drives early epigenetic remodeling of Tex-cell-associated genes
 (A–D) WT mice were treated with anti-CD137 (3H3, 10 μg) or IgG control mAb for 5 or 18 days and splenic CD44^{hi} CD8⁺ T cell chromatin states was determined through ATAC-seq. Data from 4 mice for each condition. (A) PCA of ATAC signal on peaks detected in all conditions. (B) Venn diagram showing up and down differentially accessible regions (DARs) from the indicated pairwise comparisons. (log₂FC > 2 and adj p < 0.01.) (C) ATAC signals around up and down DARs (-1.5 kb +1.5 kb) for each sample. (D) GSEA between the indicated signatures and the day 18 anti-CD137 condition.

- (E) Heatmap showing log-normalized ATAC-seq signal in the peaks overlapping the indicated Tex cell subset's genes as in Figure 2J.
- (F) ATAC signals across the *Pdcd1*, *Lag3*, and *Havcr2* loci. Previously described Tex-specific peaks are highlighted in gray.
- (G) Graph showing the transcription factor (TF) that account for the variability in chromatin accessibility between anti-CD137 and Ig conditions identified using chromVar package.
- (H) Heatmap showing for each TF the deviation score in each sample calculated with chromVar. Only TF with a variability >10 and an adj p < 0.01 were selected.
- (I) *Cd4^{cre} Cd137^{fl/fl} (Cd137^{-/-})* and *Cd45.1 (Cd137^{+/+})* mixed BM chimera were injected s.c. with B16K1 melanoma cells. Expression of Tox on tumor-infiltrating CD8⁺ memory T cells.
- (J and K) CD45.1 CRISPR-Cas9 control and CD45.2 CRISPR-Cas9 Tox-deficient CD8⁺ T cells were injected i.v. into *Rag2^{-/-} Il2rg^{-/-}* mice. After 7 days, mice were treated with anti-CD137 (10 µg; 3H3, i.p. twice a week) or IgG. (J) Experimental design. (K) Expression of the indicated markers on splenic CD8⁺ T cells. Data are presented as mean ± SEM from at least 2 independent experiments. Each symbol represents an individual mouse. *p < 0.05; **p < 0.01, ***p < 0.001 (paired t test).

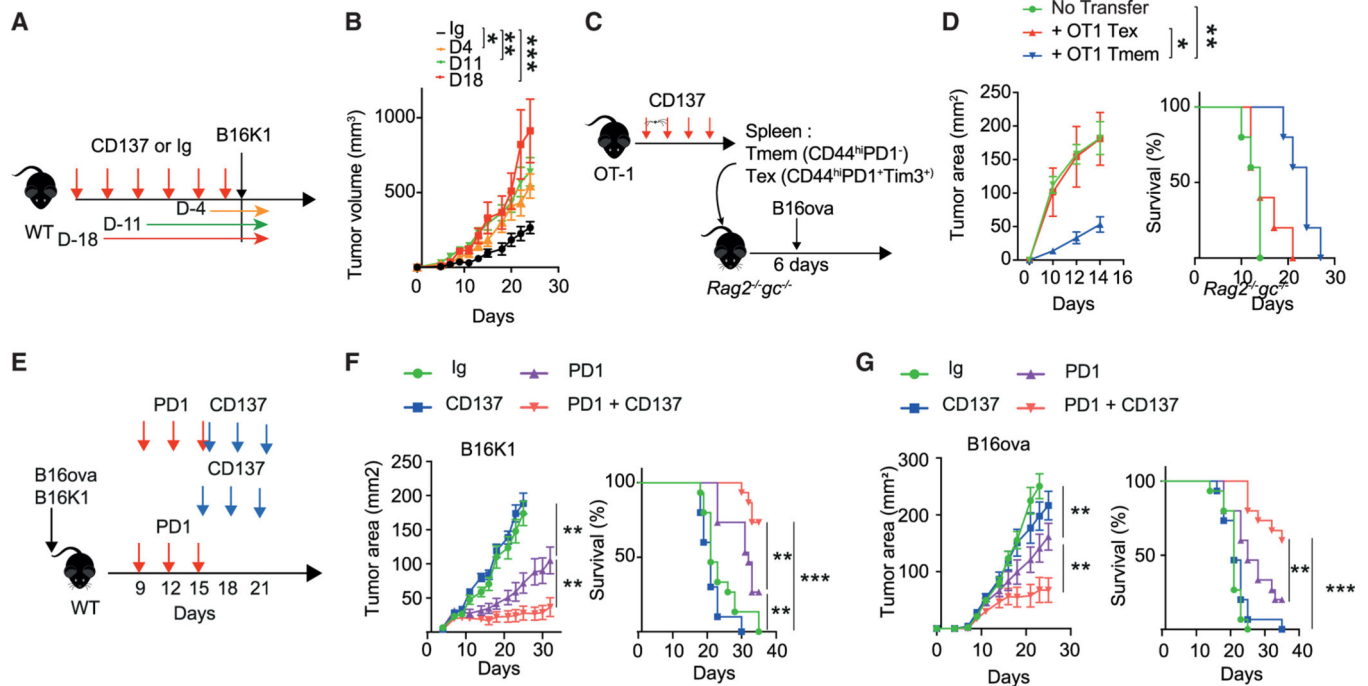


Figure 7. Contrasting effect of anti-CD137 on immune surveillance and anti-PD1 efficacy

(A and B) C57BL/6 WT mice were treated with anti-CD137 (10 μ g; 3H3, i.p. twice a week) or control IgG for the indicated period. Experimental design (A) and tumor volumes (B). (n = 5/group).

(C and D) Spleen Tmem and Tex cells were FACS sorted from OT-1 mice treated with anti-CD137 (100 μ g; 3H3, i.p. twice a week) for 18 days and transferred into *Rag2^{-/-}Il2rg^{-/-}* mice subsequently injected with B16-ova tumor cells. (C) Experimental design. (D) Tumor area and survival of the indicated groups of mice. (n = 5 mice per group from one experiment.)

(E–G) C57BL/6 WT mice were injected with B16K1 (F) or B16-ova (G) and were treated from day 9 with IgG control, anti-CD137 (10 μ g; 3H3, i.p. twice a week), anti-PD1 (250 μ g i.p., RMP1–14) or both. (E) Experimental design. (F and G) Tumor area and survival of the indicated groups of mice. (n = 10–15/group). Unless otherwise specified, data are presented as mean \pm SEM from at least 2 independent experiments. Each symbol represents an individual mouse. *p < 0.05; **p < 0.01, ***p < 0.001 (Mann-Whitney, Mantel-Cox log rank or ANOVA with Tukey's post-test analysis).

KEY RESOURCES TABLE

REAGENT or RESOURCE	SOURCE	IDENTIFIER
LEAF™ Purified anti-mouse CD3e Antibody	Biolegend	Cat#: 100331 RRID:AB_11150783
LEAF™ Purified anti-mouse CD28 Antibody	Biolegend	Cat#: 102112 RRID:AB_11150408
Anti-mouse B220/CD45R (RA3–6B2)	Biolegend	Cat:103206 RRID:AB_2174262
Anti-mouse CD3-BV421 (145–2C11)	BioLegend	RRID:AB_960120
Anti-mouse CD107a-PeCy7 (eBio1D4B)	Biolegend	Cat#: 121619 RRID:AB_657556
Anti-mouse CD138-BV421 (281–2)	BD Biosciences	Cat#: 740033 RRID:AB_394999
Anti-mouse CD138-BUV373 (281–2)	BD Biosciences	Cat#: 564430 RRID:AB_394999
Anti-mouse CD8-BUV395 (53–6.7)	BD Biosciences	Cat#: 563786 RRID:AB_962672
Anti-mouse CD8-APC (53–6.7)	BD Biosciences	Cat#:560516 RRID:AB_962672
Anti-mouse CD8-BV421 (53–6.7)	BD Biosciences	Cat#: 563898 RRID:AB_962672
Anti-mouse CD8-PeCy7 (53–6.7)	BD Biosciences	Cat#: 561097 RRID:AB_962672
Anti-mouse CD62L-BV605 (MEL-14)	BioLegend	Cat#: 104437 RRID: AB_11125577
Anti-mouse TCR Vbeta 5.1 5.2 TCR-BUV737 (MR9–4)	BD Biosciences	Cat#: 748931; RRID:AB_2873334
Anti-mouse TCR Valpha2-eFluor 450 (B20.1)	Thermo Fisher Scientific	Cat#: 48–5812-82 RRID: AB_10804752
Anti-mouse CD45.2-BUV395 (104)	BD Biosciences	Cat#: 564616 RRID: AB_2738867
Anti-mouse CD44-FITC (IM7)	BioLegend	Cat#: 103006 RRID: AB_312957
Anti-mouse CTLA-4-BV421 (UC10–4B9)	BioLegend	Cat#: sc-53682 RRID:AB_628930
Anti-mouse LAG3-PercPCy5.5 (eBioC9B7W)	Thermo Fisher Scientific	Cat#: 46–5882-80 RRID:AB_494216
Anti-mouse Tbet-Pecy7 (4B10)	Thermo Fisher Scientific	Cat#: 25–5825-82 RRID:AB_11042699
Anti-mouse Tim3-Pecy7 (RMT3–23)	Thermo Fisher Scientific	Cat#:432910 RRID: AB_2573483
Anti-mouse TNF-PercPCy5.5 5 (MP6-XT22)	BD Biosciences	Cat#: 560659 RRID: AB_1727580
Anti-mouse KI67-PerCPeFluor710 (SOLA15)	Thermo Fisher Scientific	Cat#: 56–5698-82 RRID:AB_11040981
Anti-Mouse Ly-108 (SLAMF6) Pacific Blue [clone: 330-AJ]	BioLegend	Cat#: 134608; RRID: AB_2188093
Anti Mouse Ly-108 BUV395 [13G3]	BD Biosciences	Cat#: 745730; RRID:AB_2743205
Anti-Human/anti-Mouse TCF1/TCF7 AF647 [C63D9]	Cell Signaling Technology	Cat#: 14456S
Anti-human/mouse Tcf1/tcf7 AF488 [C63D9]	Cell Signaling Technology	Cat#: 6444S

REAGENT or RESOURCE	SOURCE	IDENTIFIER
Anti-human/Anti-Mouse TCF1/TCF7 PE [C63D9]	Cell Signaling Technology	Cat#: 6709S
Anti-mouse CD45.1-FITC (A20)	BD Biosciences	Cat#: 110706 RRID: AB_313495
Anti-mouse TCRb-Perc PCy5.5 (H57-597)	BioLegend	Cat#:109228 RRID: AB_1575173
Anti-mouse CD155 (PVR) PE (TX56)	BioLegend	Cat#:131508 RRID: AB_1279107
Anti-mouse TIGIT-PeCy7 (1G9)	BioLegend	Cat#:142108 RRID: AB_2565649
Anti-mouse TIGIT-APC (1G9)	BioLegend	Cat#: 142105; RRID: AB_10962572
Anti-mouse Eomes-efluor660 (DAN11MAC)	Thermo Fisher Scientific	Cat#:50-4875-80 RRID: AB_2574227
Anti-mouse Ki67-AF700 (SOLA15)	Thermo Fisher Scientific	Cat#:56-5698-92 RRID: AB_2637480
Anti-mouse Eomes-EF450 (DAN11MAC)	Thermo Fisher Scientific	Cat#:48-4875-82 RRID: AB_2574062
Anti-mouse IFNg BV421 (XMG1.2)	BD Biosciences	Cat#: 505830 RRID: AB_2563105
Anti-mouse CD226-BV421 (TX42.1)	BioLegend	Cat#:133615 RRID: AB_2715977
Anti-mouse TCRb-BV510 (H57-597)	BioLegend	Cat#:109233 RRID: AB_2562349
Anti-mouse TCRb-PercPCy5.5 (H57-597)	BioLegend	Cat#:109228 RRID: AB_1575173
Anti-mouse CD62L-APC (MEL-14)	invitrogen	Cat#: 17-0621-81 RRID: AB_469410
Anti-mouse PD1 (CD279)-BV785 (29F.1A12)	BioLegend	Cat#:135225 RRID: AB_2563680
Anti-mouse PD-1	Bio X Cell	Cat#: BP0146 RRID: AB_10949053
Anti-mouse OX40	Bio X Cell	Cat#: BE0031 RRID: AB_1107592
Anti-mouse 4-1BB (CD137, 3H3)	Bio X Cell	Cat#: BE0239 RRID: AB_2687721
Anti-mouse 4-1BB (CD137, LOB12.3)	Bio X Cell	Cat#: BE0239 RRID: AB_10949016
Anti-mouse GITR	Bio X Cell	Cat#: BE0063 RRID: AB_1107688
Rat IgG2a	Bio X Cell	Cat#: BP0089 RRID: AB_1107769
Rat IgG1	Bio X Cell	Cat#: BP0169 RRID: AB_1107775
Chemicals, peptides, and recombinant proteins		
Recombinant murine IL-7	Peprotech	Cat#: 217-17
Brefeldin A Solution (1000X)	Thermo Fisher Scientific	Cat#: 00-4506-51
Golgi Plug	BD Biosciences	Cat#: 555029
Protein Transport Inhibitor	BD Biosciences	Cat#: 554724
Ionomycin	Sigma-Aldrich	Cat#: I0634
Phorboll 12-myristate 13-acetate (PMA)	Sigma-Aldrich	Cat#: P8139

REAGENT or RESOURCE	SOURCE	IDENTIFIER
RPMI Medium 1640	Thermo Fisher Scientific	Cat#: 61870-010
Fetal Bovine Serum	N/A	N/A
Ficoll® Paque Plus	Sigma-Aldrich	Cat#: 17-1440-03
Acridine Orange / Propidium Iodide (AO/PI)	Logos Biosystems	Cat#: F23001
RLT lysis buffer	Qiagen	Cat#: 79216
B-mercaptoethanol	Sigma-Aldrich	Cat#: M6250
FK506	InvivoGen	Cat#: inh-fk5-5
Cyclosporine A	InvivoGen	Cat#: ttrl-cyca
Alt-R® S.p. Cas9 Nuclease V3	IDT	Cat#: 1081059
Negative control crRNA #1	IDT	Cat#: 1072544
Critical commercial assays		
Tumor Dissociation Kit	Miltenyi Biotec	Cat#130-096-730
CD45 (TIL) microbeads, mouse	Miltenyi Biotec	Cat#: 130-110-618
RNeasy Plus Micro Kit	Qiagen	Cat#: 74034
Fixable viability dye efluor 780	Thermo Fisher Scientific	Cat#:65-0865-14
CellTrace™ Violet Cell Proliferation Kit	Thermo Fisher Scientific	Cat#:C34557
CD8+T cell isolation Kit, mouse	Miltenyi Biotec	Cat#:130-104-075
Foxp3 Transcription Factor Staining Buffer Set	Thermo Fisher Scientific	Cat#:00-5523-00
Fixation/Permeabilization Solution Kit	BD Biosciences	Cat#: 554714
TRUSEQ STRANDED MRNA HT (96 SAMPLES)	Illumina	Cat#: RS-122-2103
NEXTSEQ 500 HIGH OUTPUT KIT v2 (150cycles)	Illumina	Cat#: FC-404-2002
Chromium Single Cell 3' Library & Gel Bead Kit v3	10XGENOMICS	Cat#: 1000147
KAPA Quantification Kit	KAPABiosystems	Cat#: KK4824
Chromium Next GEM Single Cell 5' Library & Gel Bead Kit v1.1	10XGENOMICS	Cat#: 1000167
QIAGEN MinElute kit	QIAGEN	Cat#: 28004
Nextera DNA Library Prep Kit	Illumina	Cat#: FC-131-1096
Illumina Novaseq 6000 S1 Reagent Kit v1.5	Illumina	Cat#: 20028313
CBA Mouse TNF Flex Set - C8	BD Biosciences	Cat#: 558299
CBA Mouse IFN γ Flex Set - A4	BD Biosciences	Cat#: 558296
Mouse Soluble Protein Master Buffer Kit	BD Biosciences	Cat#: 558266
P3 Primary Cell 4D-Nucleofector™ X Kit S	Lonza	Cat#: V4XP-3032
Deposited data		
Transcriptomic analysis of VK12653 Multiple Myeloma bone marrow microenvironment upon treatment with anti-CD137 agonists	This paper	GEO: GSE206545
Single cell Transcriptomic analysis of CD8+ T cells treated with anti-CD137 agonists with in VK12653 Multiple Myeloma bone marrow microenvironment.	This paper	GEO: GSE205702
Single cell Transcriptomic analysis of CD8+ T cells from bone marrow chimeras reconstituted with CD137 wild-type or knock out bone marrow, and implanted with B16K1 melanoma.	This paper	GEO: GSE205703

REAGENT or RESOURCE	SOURCE	IDENTIFIER
ATACseq analysis of sorted CD44hiCD8+ T cells isolated from the spleen of C57BL/6 mice treated with aCD137 or an Ig control.	This paper	GEO: GSE228271
Single-cell transcriptomic analysis of sorted CD8+ T cell subsets isolated from the spleen of C57BL/6 mice treated with aCD137 or an Ig control	This paper	GEO: GSE230626
Longitudinal single cell transcriptional mapping of effector, memory, and exhausted CD8 T cells reveals shared biological circuits across distinct cell fates	Giles et al. ⁵²	GSE199565; PMID: 36271148
CD8 TILs from patients with metastatic melanoma	Lucca et al. ⁴⁷	dbgap phs002289.v1.p1 PMID:33651881 http:// biokey.lambrechtslab. org .
CD8 TILs from patients breast cancer	Bassez et al. ⁴⁸	PMID:33958794
10X single-cell RNASeq profiling of tumor-infiltrating CD8+ T-cells from B16-OVA mouse melanoma tumors	Miller et al. ⁴¹	GSE122675 PMID: 30778252
10X single-cell RNASeq profiling of GP33-tetramer+ CD8+ T-cells from mice chronically infected with LCMV Clone 13	Miller et al. ⁴¹	GSE122712 PMID:30778252
D8 p.i. single cell RNA Sequencing on P14 cells	Chen et al. ¹⁰	GSE131535; PMID:31606264
Experimental models: Cell lines		
Mouse: B16K1	Gift from Dr Segui B.	Porgador et al. ⁸⁷
Mouse: B16F10	ATCC	Cat#: CRL-6475
Mouse: MC38	Gift from C.Devaud	Trimaglio et al. ⁸⁸
Mouse: B16F10 that express constitutively OVA	Gift from B.Segui	Weulersse et al. ²⁴
Mouse: Vkmyc12653	Gift from L.Bergsagel	Chesi et al. ⁸⁹
Experimental models: Organisms/strains		
C57BL/6 alias WT	Jackson Laboratory	Cat#: SC-C57J-F
B6.SJL-Ptprca Pepcb/BoyJ alias CD45.1	Janvier Laboratory	RRID: IMSR_JAX:002014
B6-Tg(TcrαTcrβ)1100Mjb/J alias OT-1	Jackson Laboratory	Cat#: 003831
B6-CD137 ^{fl/fl} x Cd4 ^{CRE}	Gift from B.Salomon	First description
B6-ROSA26 ^{tomato} Cd137 ^{fl/fl} x Cd4 ^{CRE}	Gift from B.Salomon	First description
C57BL/6-Rag2 ^{-/-} Il2rg ^{-/-}	Jackson Laboratory	RRID: IMSR_JAX:014593
B6.IFNGR1 ^{-/-}	Jackson Laboratory	RRID: IMSR_JAX:003288
B6.Ifnar ^{-/-}	Jackson Laboratory	RRID: MMRRC_032045- JAX
B6.II12p40 ^{-/-}	Jackson Laboratory	RRID: IMSR_JAX:002693
B6.II18 ^{-/-}	Gift from K.Nakamura	Nakamura et al. ⁹⁰
B6.II6 ^{-/-}	Jackson Laboratory	RRID: IMSR_JAX:002650
B6.Tnf ^{-/-}	Jackson Laboratory	RRID: IMSR_JAX:005540

REAGENT or RESOURCE	SOURCE	IDENTIFIER
B6.II10 ^{-/-}	Jackson Laboratory	RRID: IMSR_JAX:002251
B6.II1r ^{-/-}	Gift from K.Nakamura	Nakamura et al. ⁹⁰
B6.II27ra ^{-/-}	Jackson Laboratory	RRID: IMSR_JAX:018078
B6.Cc15 ^{-/-}	Jackson Laboratory	RRID: IMSR_JAX:005090
B6.B2m ^{-/-}	Jackson Laboratory	RRID: IMSR_JAX:002087
B6.Rel ^{fl/fl} x Cd4 ^{CRE} mice	Gift from Y. Grinberg-bleyer	Grinberg-Bleyer et al. ⁶⁶
B6.Re1 ^{fl/fl} x Cd4 ^{CRE} mice	Gift from Y. Grinberg-bleyer	Grinberg-Bleyer et al. ⁶⁶
B6.Relb ^{fl/fl} x Cd4 ^{CRE} mice	Gift from Y. Grinberg-bleyer	Lalle et al. ⁶⁸
B6.Nfkb2 ^{fl/fl} x Cd4 ^{CRE} mice	Jackson Laboratory	RRID: IMSR_JAX:028720
B6.Traf1 ^{-/-}	Gift from T. Watts	RRID: IMSR_JAX:008076
Recombinant DNA		
Mm.Cas9.TOX.AA - AACCGGATTCTACCTCATTC	IDT	N/A
Mm.Cas9.TOX.AB - GATCACGGTGTCCAACATGC	IDT	N/A
Mm.Cas9.TOX.AC - TTTGTTCTTTTCGTGATACCC	IDT	N/A
Software and algorithms		
Graphpad Prism 9.3.1 software	GraphPad Software, Inc.	http://www.graphpad.com/scientific-software/prism/
FlowJo V10	FlowJo LLC	www.flowjo.com
Alignment	STAR (version 2.3.0)	Dobin et al. ⁹¹
Gene expression	Subread featurecount OUTPUAlgorithm (version 1.4.6)	Liao et al. ⁹²
Gene expression normalization	limma R package	Ritchie et al. ⁹³
ScRNAseq alignment	Cellranger v6.1.2	10x Genomics
ScRNAseq data editing and tidying	Tidyverse v1.3.2	https://github.com/tidyverse/tidyverse/releases
ScRNAseq data visualization	ggsignif v0.6.3	https://github.com/const-ae/ggsignif/releases
ScRNAseq data visualization	ggforce v0.4.1	https://github.com/thomasp85/ggforce/releases
ScRNAseq data visualization	ggraph v2.1.0	https://github.com/thomasp85/ggraph/releases
ScRNAseq data visualization	Viridis v0.6.2	https://github.com/sjmgarnier/viridis/releases

REAGENT or RESOURCE	SOURCE	IDENTIFIER
ScRNAseq data visualization	ggsci v2.9	https://github.com/nanxstats/ggsci/releases
ScRNAseq statistical analysis	broom v1.0.0	https://broom.tidymodels.org/news/index.html
ScRNAseq statistical analysis	rstatix v0.7.0	https://github.com/kassambara/rstatix
ScRNAseq statistical analysis	matrixStats v0.62.0	https://github.com/HenrikBengtsson/matrixStats
ScRNAseq gene annotation	biomaRt v2.50.3	https://cran.r-project.org/web/packages/biomaRt/biomaRt.pdf
ScRNAseq toolkit	Seurat v4.0.0	https://satijalab.org/seurat/
ScRNAseq batch correction	harmony v0.1.0	https://cran.r-project.org/web/packages/harmony/index.html
ScRNAseq differential gene expression analysis	presto v1.0.0	https://www.biorxiv.org/content/10.1101/653253v1.full.pdf
TcR repertoire analysis	scRepertoire v1.7.2	Borcherding et al. ⁶²
TcR repertoire analysis	Trex v0.99.9	https://github.com/ncborcherding/Trex
ATACseq base trimming	TrimGalore v0.6.5	N/A
ATACseq alignment	STAR v2.6.0c	N/A
ATACseq raw data manipulation	samtools v1.9	https://github.com/samtools/samtools
ATACseq raw data manipulation	picard v1.88	https://github.com/broadinstitute/picard
ATACseq peak calling	MACS2 v2.1.0.20150731	https://pypi.org/project/MACS2/
ATACseq data exploration	deeptools v3.3.1	https://deeptools.readthedocs.io/en/latest/
ATACseq quantile normalization	ChiPin v0.1.0	Polit et al. ⁹⁴
ATACseq peak signal quantification	MegaDepth v1.8.0	https://github.com/zhengqili/MegaDepth
ATACseq differential peak abundance analysis	DESeq2 v1.38.3	Love et al. ⁹⁵
ATACseq signal visualization	pyGenomeTracks v3.8	https://pygenometracks.readthedocs.io/en/3.8/
ATACseq peak structural annotation	HOMER v4.10.4	http://homer.ucsd.edu/homer/
ATACseq motif analysis	chromVar v1.20.20	Schep et al. ⁷¹
ATACseq motif analysis	Motifmatchr v1.20.20	Schep et al. ⁷¹